QT-Interval Adaptation to Changes in Autonomic Balance

by

Ehimwenma Nosakhare

B.S., Electrical Engineering, Howard University, 2011

Submitted to the Department of Electrical Engineering and Computer Science
in partial fulfillment of the requirements for the degree of

Master of Science
in Electrical Engineering and Computer Science
at the Massachusetts Institute of Technology

September 2013

Signature of Author: _____
Department of Electrical Engineering and Computer Science
August 30, 2013

Certified by: _____
George C. Verghese
Henry Ellis Warren (1894) Professor of Electrical and Biomedical Engineering
Thesis Supervisor

Certified by: _____
Thomas Heldt
Assistant Professor of Electrical and Biomedical Engineering
Thesis Supervisor

Accepted by: _____
Leslie A. Kolodziejski
Professor of Electrical Engineering and Computer Science
Chair, Committee for Graduate Students

QT-Interval Adaptation to Changes in Autonomic Balance

by Ehimwenma Nosakhare

Submitted to the Department of Electrical Engineering and Computer Science
in partial fulfillment of the requirements for the degree of
Master of Science

Abstract

ECG variability, as it relates to the influence of the autonomic nervous system on the heart, is primarily studied via frequency-domain and time-domain analysis of heart rate variability (HRV). HRV studies the variability of the RR intervals in the ECG; these intervals are modulated by the autonomic influence on the periodicity of the the heart's pacemaker, the sino-atrial node. The autonomic influence at this level is dominated by the parasympathetic nervous system. In order to have a robust assessment of autonomic balance, there is a need for an ECG-based approach to assess the influence of the sympathetic nervous system. In this thesis, using spectral analysis, we quantify the variability of the QT interval, which is primarily modulated by the sympathetic nervous system. We also estimate the time constant of the sympathetic nervous system by least-squares fitting of the QT time series resulting from step perturbations in autonomic balance. This study is carried out on graded head-up tilt test data. Our results demonstrate the potential of QT interval variability as a non-invasive assessment of the sympathetic nervous system activity on the heart.

Thesis Supervisor: George C. Verghese
Title: Henry Ellis Warren (1894) Professor of Electrical and Biomedical Engineering

Thesis Supervisor: Thomas Heldt
Title: Assistant Professor of Electrical and Biomedical Engineering

Acknowledgments

Ponder anew what The Almighty can do, if with His love He befriends thee....
To God be the glory, great things He has done!

I would like to thank several of my mentors who have provided tremendous support and encouragement towards the completion of this work. I thank Professor George Verghese for patiently teaching me how to become a researcher. His constant reminder to "always do those sanity checks" have made me think even more critically about my research. I thank Professor Thomas Heldt for teaching me the much needed physiology background for this thesis, for providing solutions to the problems I encountered with the QT detection algorithm and for his tilt table data. Thanks also go to Dr. Robert Tasker of Boston Children's Hospital for sparking this project and his continued guidance on it.

My family has also contributed to the success of this thesis. To mum and dad, you are amazing parents. Thank you for believing in me and supporting me in my academic pursuits, and in my life in general. I could not have done this without you both. And mum, you can now add another degree to your name. To my four wonderful sisters: Esosa, Adesuwa, Nosariemen and Osato, you ladies are the best! Thank you for your unwavering support, love and friendship.

Ayobami, your name says it all, your love, friendship and prayers are beyond what I could have asked for. Thank you for providing the motivation and encouragement needed to complete this thesis and also for the constant reminder to eat! Chioma and Tayo, thank you for allowing me into your home. I am extremely grateful for your many words of encouragement, your prayers and the laughs we have shared. You two are my favorite couple, and your friendship means a lot to me. Karen and Lois, thank you for your indispensable friendship and support over the years. To my other friends too many to mention, thank you for making my time here at MIT worthwhile.

I cannot end without thanking the people who make up my support network here at MIT. Monica Orta, thank you for always listening to me and giving me a hug when-

ever I need one. You are a very reliable friend and you truly have the best interests of people at heart. The MIT Summer Research Program (MSRP) is so lucky to have you. Janet Fischer, I doubt my MIT journey would have started if you did not reach out to me at CONVERGE. I am grateful for how you always answer my many administrative questions, and ease me of my concerns. For these and many other things, I thank you. Mary Thompson, thank you for the prayer sessions, you are amazing! I would also like to thank the Computational Physiology and Clinical Inference group (CPCI), the MIT Graduate Christian Fellowship (GCF) and my MSRP family.

I thankfully acknowledge financial support from Dr Robert Tasker and the Boston Children's Hospital Anesthesia Foundation, the EECS Great Educator Fellowship Fund from the Department of Electrical Engineering and Computer Science, and my parents.

Contents

List of Figures

List of Tables

Chapter 1

Introduction

AN electrocardiogram (ECG) is a graphical recording of the electrical activity of the heart muscle over time. The electrical system of the heart, also known as the cardiac conduction system, controls the events that occur as the heart expands to fill up with blood and contracts to pump blood throughout the body. The electrical impulses generated within the heart muscle are detected by electrodes placed on the surface of the skin, and connected by leads to the ECG machine.

Different types of ECG exist and are referred to by the number of leads that are recorded. There are 3-lead, 5-lead and the 12-lead ECGs. The standard 12-lead ECG used in clinical practice to make recordings consists of six frontal and six precordial leads placed on each arm, each leg and across the chest. The machine can be found in hospitals and ambulatory settings. The advancement of technology has now allowed for portable ECG machines to be attached to patients as they go about their everyday activities.

In the clinical setting, the ECG has become an important diagnostic tool. It is useful in indicating if there are any irregular heart beats or heart rhythms, if the heart has enough blood, if any part of the heart is damaged or whether a heart attack has occurred or is likely to be occurring. It is also used in the diagnosis of a variety of heart

diseases including coronary heart disease, congenital heart defects and pericarditis. However, a normal ECG does not rule out serious heart disease, and this has given rise to specialized ECGs like the exercise ECG and ambulatory ECG, which are worn for 24-48 hours.

In addition to diagnostics, other information about the heart can be obtained from the ECG. For example, the reciprocal of the distance between successive dominant peaks (or R waves) of the ECG measures the instantaneous heart rate in *beats per second.* The ECG also shows the duration of the depolarization and repolarization (in the case of the ventricles) of the different chambers of the heart. The wealth of information the ECG provides has given rise to the assessment of the autonomic nervous system (ANS) influence on the heart via ECG variability. Quantifying the variability of intervals in the ECG provides a non-invasive measure of the modulation of cardiac autonomic tone.

In the literature, cardiac autonomic tone is predominantly assessed by heart rate variability (HRV). HRV is the analysis of how the heart rate varies with time, and consequently how RR intervals vary. As a result, HRV primarily measures the modulation of the parasympathetic nervous system (PNS), one of the branches of the ANS. In order to analyze to effects of the other branch of the ANS, the sympathetic nervous system (SNS), the variability of the QT intervals has to be studied.

The QT interval is one of the major intervals on the ECG. There are several reasons QT interval variability is a better assessment of SNS modulation. First, the QT interval measures the depolarization and repolarization of the ventricles, where sympathetic activity is dominant. Second, QT variability depends on autonomic inputs regulating ventricular repolarization duration independent of the heart period [29] [8]. Third, sympathetic activity has a more pronounced effect on ventricular myocardial contractility and a much smaller effect on heart rate.

In order to characterize QT interval variability, we first detect the QT intervals from the ECG by implementing a curve length transform algorithm. These detected QT intervals make up the time series data that is used in spectral analysis and time-domain classification of QT variability. To make a contrast between the effects of PNS and SNS on the QT interval, these methods are also applied to the RR intervals equally detected from the ECG. Spectral analysis provides a quantitative marker of sympathovagal balance and highlights the primary influence of the SNS on the QT interval. The time-domain analysis goes a step further and allows us to estimate the time constant of autonomic influence on the QT interval.

Analysis is done on graded head-up tilt table data, which is an experimental condition known to produce an increase of sympathetic tone and modulation according to the inclination of the tilt table. Results show that the QT interval is primarily influenced by the SNS, and QT variability has great potential to be used as a non-invasive measure of cardiac sympathetic tone.

The remaining chapters in this thesis are organized as follows. Chapter 2 presents the background information necessary to understand the effects of the ANS on the heart, why it is necessary to quantify ANS modulation, and the reason the ECG is the right tool for assessment of brain-heart interaction. The detection of the QT intervals and the results from testing the implemented algorithm are detailed in Chapter 3. Chapter 4 provides a description of the spectral analysis method and the method used in the time-domain analysis, least-squares fitting. Chapter 5 reports QT variability characterization results in both the frequency and time domain. Finally, Chapter 6 summarizes the contributions of the thesis and touches on the possible directions of future work.

Chapter 2

Background

OF all the organs in the body, the heart is one of the most monitored and studied in both the clinical and research settings. Hence, hospital acute medical care, ambulatory services and other emergency medical service providers constantly utilize cardiac monitors to assess patients cardiac rhythms. Technology advances have even made it possible for health care providers to monitor the heart outside of hospital settings, with patients given the opportunity to carry around event monitors.

Electrocardiograpy is the primary way of cardiac monitoring. It consists of using a machine to produce a graphical recording of the electrical activity of the heart, called an electrocardiogram (ECG). This record highlights changes in a patient's heart condition and helps to aid diagnosis.

The first use of electrocardiography in humans dates back to 1885 when Augustus D. Waller first recorded the heart's electrical activity. However, Dr. Willem Einthoven, a Dutch physiologist and Nobel laureate, coined the term "electrocardiogram" in 1893 [3]. Ever since, the ECG has been used as a first-line diagnostic tool, and health care providers at different levels find it necessary to interpret the ECG. The ECG has helped in the diagnosis of various forms of heart disease, especially arrhythmias (abnormal heart rhythms), acute myocardial infarction and ischemic heart disease.

The use of the ECG has now gone beyond clinical diagnostics of arrhythmic heart disease. The ECG can provide information about heart rate, and since heart rate is influenced by the autonomic nervous system (ANS) [26], information from the ECG can be harnessed to investigate cardiac autonomic tone.

■ 2.1 Cardiovascular Physiology

The major function of the heart is to pump blood around the body, carrying oxygen and nutrients to organs, muscles and tissues, and transporting waste such as carbon dioxide to the lungs for expiration. It accomplishes this task by expanding its muscles to fill up with blood, and contracting to push out blood from the chambers within its walls.

The heart is divided into four chambers (see Figure 2.1). The upper and lower chamber on each side of the heart are called the atrium and ventricle respectively. The heart also has two pumps arranged in series, which by generating pressure, pump blood through the blood vessels to the body. Each pump is made up of an atrium and a ventricle. The right heart (one of the pumps) drives de-oxygenated blood through the lungs and back to the heart; this is the pulmonary circulation. The left heart, the other pump, drives oxygenated blood around the body; this is the systemic circulation. The coordination of these rhythmic mechanical contractions and expansions is provided by an electrical signal conducted throughout the heart muscles.

■ 2.1.1 Electrophysiology of the Heart

The cardiac cycle is the term used to describe the relaxation and contraction that occur periodically as the heart works to pump blood through the body. In order for

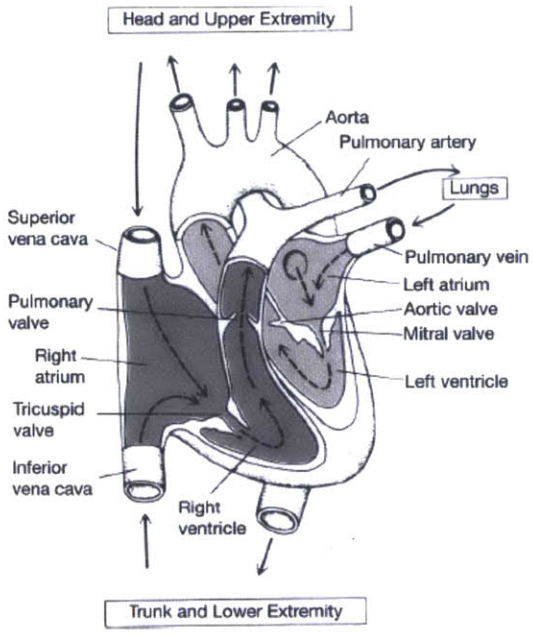

Figure 2.1: Diagram of the heart showing the four chambers, major blood vessels and direction of blood flow [16].

the heart to effectively act as a pump, the ventricular muscles have to be electrically activated and then contract. The presence of any form of disturbances in the heart's electrical activity can cause significant abnormalities in its mechanical function. In fact, malfunction of the heart's electrical behavior is the principal cause of sudden cardiac death [16]. Cardiac electrophysiology includes all of the processes involved in the electrical activation of the heart: the cardiac action potentials; the conduction of action potentials along specialized conducting tissues; the electrocardiogram (ECG); and the modulating effects of the autonomic nervous system on heart rate [10].

The heart has the ability to create its own electrical impulses or action potentials, and to control the route the impulses take via a specialized conduction pathway. The pathway includes the sino-atrial (SA) node, atrio-ventricular (AV) node, the bundle of His, the left and right bundle branches and the Purkinje fibres (as shown in Figure 2.2).

The action potential originates in the SA node, which is located just below the superior vena cava on the right atrium. The SA node is made up of conducting cells which are specialized muscle cells that spread action potentials rapidly over the entire heart muscle. The SA node serves as the pacemaker of the heart. During normal sinus rhythm (i.e., when the pattern and timing of the action potential are normal), the SA node sets the sequence and timing for the conduction of action potentials to the rest of the heart.

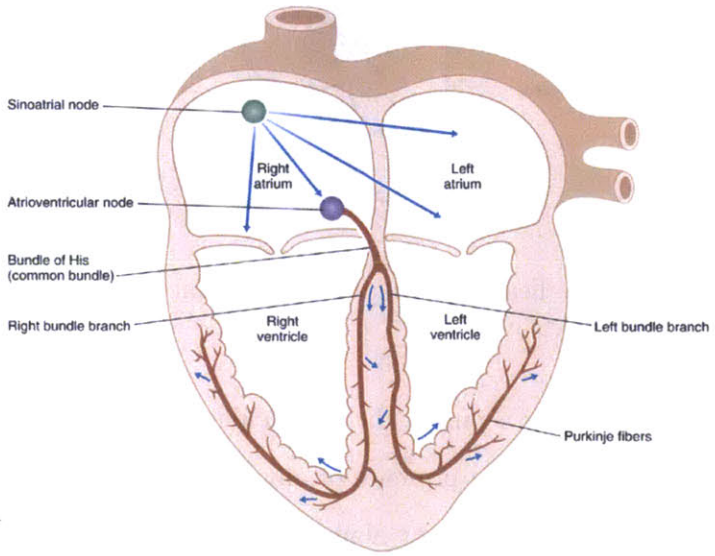

Figure 2.2: Schematic showing the conduction pathway through the heart [10].

The conduction then goes through the AV node while it is simultaneously conducted throughout the atria. The AV node is located at the base of the atria. Conduction through this node is slower than through any other cardiac muscle. This slow conduction gives the ventricles enough time to fill up with blood before they get activated to contract. When the action potential exits the AV node, it goes through the ventricular conducting system, starting with the bundle of His. Afterwards, it goes through the left and right bundle branches, and then the smaller bundles of the Purkinje system. Conduction through the ventricular conduction system is very fast. This is necessary

for efficient contraction and ejection of blood from the ventricles.

■ 2.1.2 Cardiac Action Potential

The cardiac action potential varies in form across the cells of the SA node, atrium, and ventricle. In general there are have five different phases. The ventricular action potential displays the numbered phases in Figure 2.4. The phases are made up of an initial interval of depolarization, when there is a high inflow of current into the cell membrane, and intervals of repolarization, when there is an outflow of current from the cell membrane. Phase 0 or upstroke is the phase of rapid depolarization; at its peak, the membrane is depolarized to about $+20\ mV$ (by convention, intracellular potential is expressed relative to extracellular potential, i.e., inside potential minus outside potential). Phase 1 or initial repolarization is a brief period of repolarization that immediately follows the upstroke. Phase 2 or plateau occurs immediately after phase 1. The plateau is a long period of relatively stable depolarized potential, when there is no net current flow. At phase 3, repolarization begins gradually and then moves rapidly to the resting potential. Phase 4 is the resting membrane potential; it occurs after the membrane potential fully depolarizes in phase 3 and returns to a resting level of about $-85\ mV$. In phase 4, the membrane potential is stable again and there is no net flow of currents. In the SA node, phases 1 and 2 are absent, resulting in a shorter action potential duration.

■ 2.2 The Electrocardiogram (ECG)

One of the most important and oldest tools for assessing the cardiac conduction system is the ECG. As the action potential moves through the heart, an electric potential field is generated, and this field can be measured by electrodes placed on the body surface.

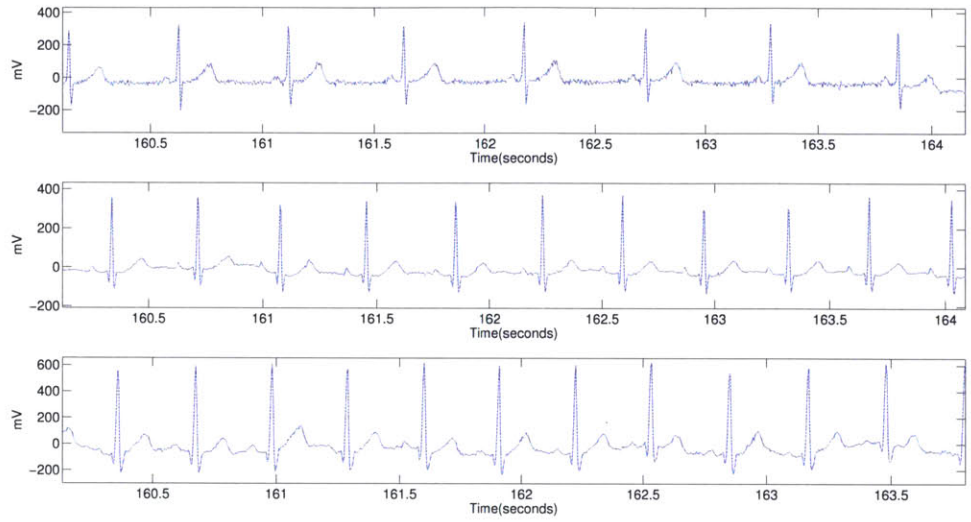

Figure 2.3: Continuous ECG tracings showing normal sinus rhythm (NSR) in three different patients [17].

The sequence of depolarization and repolarization of the heart makes it possible to measure this potential difference on the body surface. The entire heart does not depolarize at the exact same time; the depolarization occurs in sync with the phases of the action potential through the heart muscles. As a result, the atria depolarize before the ventricles; the ventricles depolarize in a particular sequence; the atria repolarize while the ventricles are depolarizing; and the ventricles repolarize in a particular sequence.

The ECG is made up of different wave segments as well as isoelectric segments during which either no electric activity is detected or the chambers of the heart remain depolarized. The prominent wave segments of the ECG are the P-wave, the QRS complex (consisting of the Q, R and S waves) and the T-wave, see Figure 2.4. The P-wave represents the change in voltage on the body's surface as the atrium gets depolarized, the QRS complex represents ventricular depolarization, and the T-wave represents ventricular repolarization. The atrial repolarization wave occurs but it is buried under

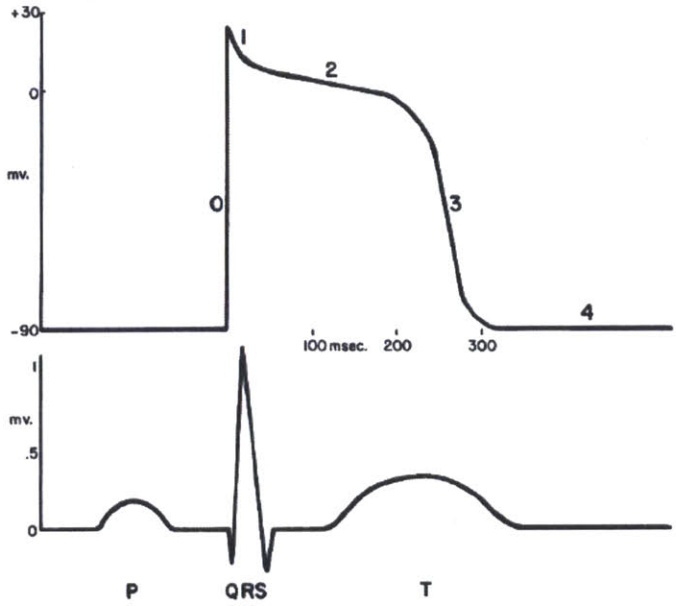

Figure 2.4: Sketch of a ventricular action potential (*above*) and corresponding typical single electrical ECG event (*below*) [16].

the QRS complex and its not identifiable on the ECG. The PQ segment, which is the isoelectric segment after the P wave and before the QRS complex, represents the time the action potential travels through the AV node and ventricular conduction system. The ST segment corresponds to the plateau period of the action potential during which the ventricles remain depolarized.

An important interval measured on the ECG is the RR interval, from which heart rate is derived ($HR = \frac{1}{RR}$) and heart rate variability (HRV) is studied (see Subsection 2.4.1). This interval is measured as the distance between successive R waves (se Figure **??**). Another important interval, the QT interval, is measured from the start of the QRS complex until the end of the T-wave. The QT inteval captures the electrical activity during depolarization and repolarization of the ventricles.

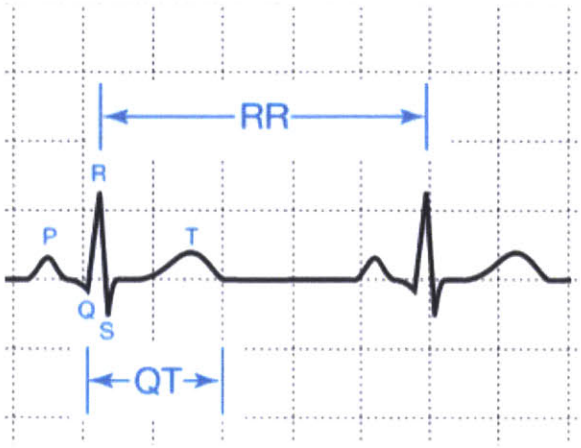

Figure 2.5: Mock ECG showing measurement of QT and RR interval. Adapted from Al-Khatib *et al* [2].

■ 2.3 Neural Regulation of the Cardiovascular System

Neural regulation of the cardiovascular system is effected through the parasympathetic (PNS) and sympathetic (SNS) nervous system. They are known to be the principal systems involved with short-term cardiovascular control, on the time scale of 0.5 - 30 seconds.These two systems make up the autonomic nervous system (ANS). One of the functions of the ANS is to increase and decrease the workload of the heart depending on the requirements of the body. In most physiologic conditions, the outflow of either the PNS or SNS is closely followed by the inhibition of the other.

The PNS predominates in resting conditions and has a restorative function; it always tries to conserve energy. When activated, the effects of the PNS are seen more rapidly. The major site of action of the PNS on the heart is the SA node. When activated, it decreases heart rate, in contrast to SNS. It also has mild inhibitory effects on the contractile force of the heart [24].

The SNS on the other hand, gets the body ready for activity. It is activated during

stressful conditions and generates a "fight or flight" response. One of the primary effects of the SNS on the heart is the stimulation of the heart muscles, thereby increasing the contractility of the muscles in both the atria and ventricles. Another effect is the increasing heart rate.

The SA node, the primary pacemaker of the heart, has both both sympathetic and parasympathetic innervations. However, the SNS does not provide a constant input to the sino-atrial node during resting conditions, whereas the PNS does.

■ 2.3.1 Sympathetic Effects on the QT Interval

The primary neurotransmitter of the SNS is norepinephrine (NE). When the SNS is activated, NE acts on receptors located in the heart. To increase cardiac contractility, the SNS acts through a collection of nerve cells called the left stellate ganglion that act directly on the left ventricle through NE and β-adrenergic receptors (the receptor in the heart that is concerned with the increase of contractility of the heart muscles). The SNS therefore has a direct effect on the ventricles and consequently, the QT interval (see Figure 2.6).

■ 2.4 ECG Variability

The different intervals on the ECG vary with time. This is as a result of autonomic control, breathing and other regulatory systems in the body, like the Renin-Angiotensin system and thermoregulatory control. Various studies have established and quantified the variability of the RR intervals, through heart rate variability, and the variability of the QT intervals. The following subsections discuss the variability of these intervals as assessed in the literature.

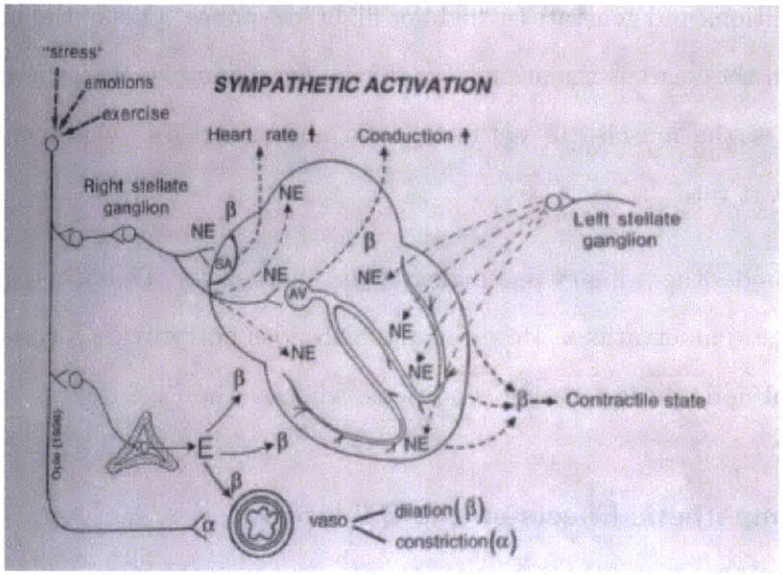

Figure 2.6: Diagram showing the mechanism of sympathetic stimulation [24]. The left stellate ganglion of the SNS releases NE to the left ventricles, which activates the β-adrenergic receptors and causes an increase in contractility of the heart.

■ 2.4.1 Prior Analysis: Heart Rate Variability

Heart rate variability (HRV) is a measure of how the heart rate varies under the action of the ANS. Analyzing HRV in the time or frequency domain is one of the important non-invasive assessments of the modulation of heart frequency by the sino-atrial node (SA node). The dynamics of HRV serve as an indicator of how heart rate, respiration and blood pressure are controlled by the body.

Under normal physiologic conditions, variability in heart rate is related to the two phases of respiration. The heart rate increases with inspiration and decreases with expiration. This rapid adjustment is primarily mediated by the PNS. Feedback mechanisms for regulating temperature and blood pressure are also responsible for the variation of heart rate.

The clinical importance of HRV as an indicator of mortality has been established

as early as 1965 [34]. Cardiac abnormality can be associated with decreased heart rate variability and thus, heart rate variability has been studied with the purpose of diagnosing and predicting cardiovascular diseases. Some clinical diagnostic uses of HRV include prediction of risk after acute myocardial infarction [28][32][38], an early warning sign of diabetic neuropathy [27][11] and detection of congestive heart failure (CHF) [9][22].

Power spectral density (PSD) analysis is one of the major ways that HRV is analyzed in the frequency domain. It shows the distribution of the power in the instantaneous heart rate as a function of frequency. There are two major PSD analysis methods: Welch's method, which is non-parametric; and autoregressive (AR) modeling, which is parametric. AR modeling produces smoother spectral components in the presence of noise. However, it might require a complex model with a very high order. Welch's method utilizes the well known Fast Fourier Transform (FFT) algorithm for the calculation of the power spectrum. This algorithm is easy to implement (it is well developed in MATLAB) and is efficient in terms of fast processing speeds.

There are three different ranges of spectral components that have been identified as of interest in the power spectrum of HRV [34]. They are very low frequency (VLF): < 0.04 Hz, low frequency (LF): $0.04 - 0.15$ Hz and high frequency (HF): $0.15 - 0.4$ Hz. HRV studies have shown that PNS activity and respiratory activity can be quantified by the power in the high frequency region, while the low frequency region quantifies both the SNS and PNS response [1]. The physiological explanation of the VLF is much less defined in the literature. It is important to note, however, that the various spectral components measure the modulation of the tone of these activities and may not necessarily reflect the degree of the tone [21].

2.4.2 Prior Analysis: QT Variability

In the clinical setting, it is now widely accepted that the QT interval is subject to variability. QT variability has been shown to be elevated in congestive heart failure (CHF), ischemia and long QT syndrome [5], and thus accurate measurement of this interval as well as study of its variability are important.

The variability of the QT interval can be a result of biological factors, differences in autonomic tone, presence of electrolytes and drugs, inter- and intra-observer variability resulting from variations in T-wave morphology, and technical factors including the environment in which the ECG is recorded [2].

Heart rate also plays a major role among these many sources of variations, causing clinicians to adjust the duration of the QT interval by correction formulas that normalize the QT to heart rate alone. The aim of the correction is to produce an independence of the QT interval from heart rate. The major correction formula used is the Bazett formula, $QT_c = \frac{QT}{\sqrt{RR}}$. However several studies have shown that this is not necessarily well-suited to the intended uses, especially in cases of fast heart rate [2]. Other correction formulas that are widely used are the Fridericia cube root formula, $QT_c = \frac{QT}{\sqrt[3]{RR}}$, and Framingham linear regression equation [2]. Correction of the QT interval has been the subject of debate for over a decade now [19]. Although it has been agreed in the clinical setting that the QT interval should be corrected for heart rate, the best way to do this adjustment has not been determined.

In addition to possible detection of cardiac diseases, QT variability is used as a non-invasive measure of cardiac autonomic tone [25]. QT variability as a measure of beat-to-beat probe of autonomic nervous system activity has only recently attracted some popularity (in comparison to HRV studies) and is being investigated in various

physiological conditions. Several studies have quantified beat-to-beat variability in QT interval of the ECG using a QT variability index (QTVI) [5], QTVI is defined as:

$$\log_{10}\left[\frac{QT_v/QT_m^2}{RR_v/RR_m^2}\right] \tag{2.1}$$

where QT_v, RR_v are the variance of QT and RR intervals respectively, and QT_m, RR_m are the mean QT interval and mean RR interval respectively. The QTVI represents the log ratio between the QT interval and the RR interval variabilities, each normalized by their respective squared means. An increase in this index suggests an increase in QT interval variability. One issue that has arisen from the use of this index is the neglect of QT/RR hysteresis [20]. QTVI describes the variability of the QT interval for simultaneously assessed RR intervals. However the QT-RR relationship may be dependent on several past RR intervals [20].

In summary, there remains a need for a reliable quantitative measure of total cardiac autonomic tone. Left ventricular dysfunction is one of the cardiovascular abnormalities present after brain injury [13]. This and other ventricular abnormalities are responsible for ventricular arrhythmias. The availability of an easily applicable and non-invasive test that can assess ventricular autonomic regulation effected through the SNS is important. HRV study, which is the earliest and best established study of cardiac autonomic regulation, is restricted to the autonomic influence on the sinus nodal periodicity. The autonomic influence at this level is dominated by the PNS. Therefore, there is a need to be able to efficiently assess autonomic influence at the ventricular level, where SNS is more prominent. Using methods similar to HRV, the spectral characteristics of QT variability will be studied with the aim of quantifying the neural control mechanisms of the QT interval. The variability of the QT interval will also be assessed in the time domain.

Chapter 3

QT Detection and Measurement

IN spite of its well known limitations, manual measurement of the QT interval on surface ECG and its correction for heart rate still remains the standard quantitative evaluation of ventricular depolarization and repolarization clinically [23] [4]. In order to study QT variability and the effect of sympathetic tone on the QT interval, the interval lengths have to be determined from the ECG signal automatically and within a sufficiently high level of accuracy. Since the QT interval is measured as the distance between the Q-onset and the T-wave offset, these fiducial points have to be extracted from the ECG. The challenge of automated QT detection is compounded by the inherent imprecision in identifying the end of the T-wave in the ECG and the morphological variations in the ECG arising from the presence of arrhythmias (see Figure 3.1).

There are several methods of QT detection, including use of the curve length transform (CLT), template matching, wavelength-based delineator, and principal component regression [37] [6] [33] [15]. The QT detection algorithm used in this thesis was implemented in MATLAB using the curve length transform approach described in Zong *et al.* [36] for the Q onset, and the backward curve length transform as described in Zong *et al.* [37] for the T-wave offset. This approach was chosen because of the ease of implementation and insensitivity to baseline wander, wave polarity and high frequency

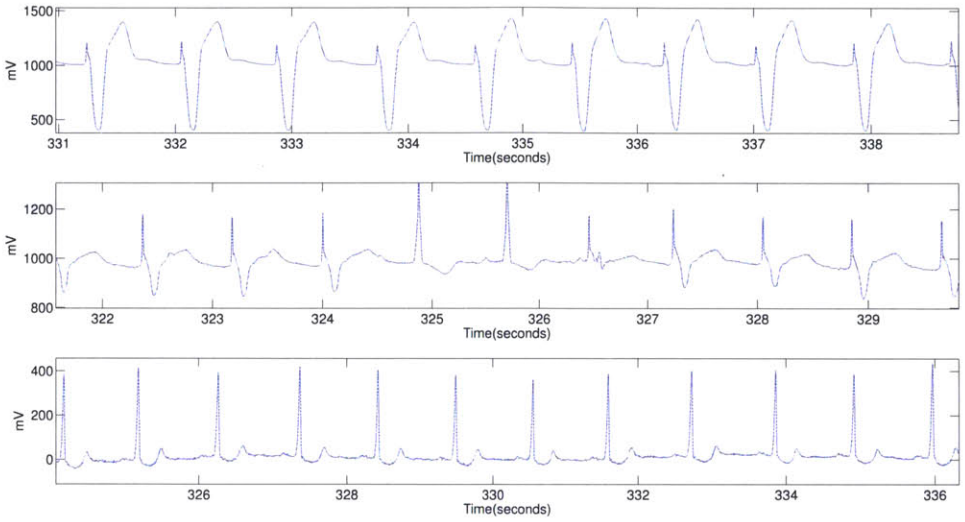

Figure 3.1: Different ECGs showing some of the various morphologies represented in the PhysioNet QT database [17], [12].

noise [37].

■ 3.1 Q-onset Detection

Given a fixed window length w, the curve corresponding to the QRS complex will have a longer length within the window than any other curve in the ECG. The ability to choose an appropriate window length characteristic of the QRS complex makes the CLT suitable for Q-onset detection.

For a differentiable function $x(t)$, the curve length transform $L(t)$ at a given time t and over a window w is given as

$$L(t) = \int_{t-w}^{t} ds = \int_{t-w}^{t} \sqrt{(1 + \frac{dx}{dt})^2} dt' \tag{3.1}$$

where ds denotes incremental length along the curve. Assuming samples x_k taken Δt

apart, the discrete time version of this is

$$L(i) = \sum_{k=i-w}^{i} \Delta t \sqrt{1 + (\frac{\Delta x_k}{\Delta t})^2} = \sum_{k=i-w}^{i} \sqrt{\Delta t^2 + \Delta x_k^2} \tag{3.2}$$

where $\Delta x_k = x_k - x_{k-1}$.

If the window length is chosen such that it corresponds to the widest QRS complex, the start of the rising edge in the transform will correspond to the Q-onset and the end of the rising edge would correspond to the S-offset. This is illustrated in Figure 3.2. Physiologically, the QRS complex should be no wider than 130 ms in healthy individuals and so the window length is set to 130 ms.

After lowpass filtering the ECG (a 3db cutoff at 16Hz), the CLT is used to detect the Q-onset and S-offset. A threshold is used for to determine whether or not a QRS complex has been found. If the threshold is crossed on any part of the CLT, the algorithm searches for the start and end of the corresponding rising edge. As suggested by Zong *et al.* [36], the start and end of the rising edge corresponds to the onset and offset of the QRS complex respectively.

■ 3.2 T-offset Detection

The detection of the T-offset is done using a variation of the CLT called the backward curve length transform (B-CLT). After the QRS portion is detected, the P-QRS portion of the filtered ECG signal is 'closed' using linear interpolation between the end points. This is to remove the QRS complex from consideration in the subsequent processing. For heart rates in the normal range, the P-QRS portion is defined as 160 ms before and after the Q-onset. The B-CLT is then calculated from a Q-onset to the Q-onset of

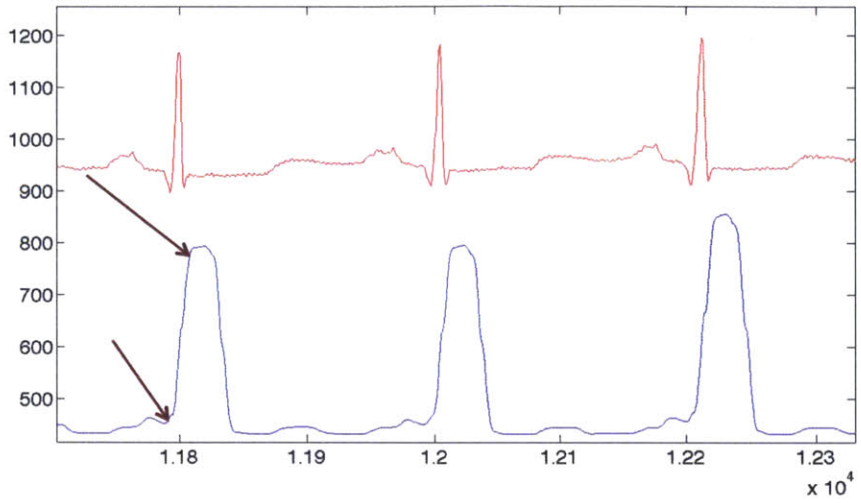

Figure 3.2: ECG and its curve length transform. Lower and upper arrow indicate the start and end of rising edge respectively.

the previous beat as follows:

$$L(i) = \sum_{k=i}^{i+w} \Delta t \sqrt{1 + (\frac{\Delta x_k}{\Delta t})^2} = \sum_{k=i}^{i+w} \sqrt{\Delta t^2 + \Delta x_k^2} \tag{3.3}$$

where $\Delta x_k = x_k - x_{k-1}$, $q_{k-1} \leq i \leq q_k$, with q_k and q_{k-1} denoting the Q-onset points for current and previously detected beats respectively. The window size w for the T-wave detection was chosen as 160 ms.

After the derivation of the B-CLT, a maximum distance search process, as described by Zong *et al.* [37], was used to determine the T-wave offset. We first contract a line from a peak point on the B-CLT signal to the Q-onset of the next beat. Moving backwards in time, the lift-off of the B-CLT corresponds to the point whose minimum distance to the constructed line is the maximum. As illustrated in Figure 3.3, this lift-off point corresponds to the T-wave offset.

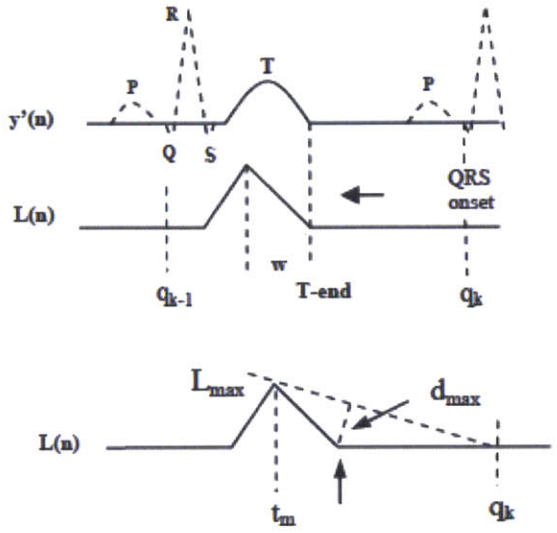

Figure 3.3: Mock ECG signal with closed P-QRS portion (*top*); Backward curve length transform signal (*middle*); Illustration of maximum distance search (*Bottom*). Adapted from Zong *et al* [37].

■ 3.3 Testing and Results

The PhysioNet QT research database serves as the reference for the validation and comparison of algorithms that extract feature annotations from ECGs [17],[12]. The database consists of a total of 105 records compiled from different PhysioNet databases. The records are selected to avoid baseline wander and other artifacts. The QT-database has a wide variety of QRS and T-wave morphologies, sufficient to challenge whatever algorithm is developed. Each record has two leads of 15 minutes of ECG sampled at 250Hz, and also has 30 - 70 beats annotated by at least one cardiologist; 11 of the 105 records were annotated by two cardiologists. In addition to the manual annotations done by the cardiologists, each record has annotations generated by an inbuilt PhysioNet detector. These automated annotations are available for the entire length of the record, i.e., 15 minutes. Only 102 records had T-wave ends annotated by a cardiologist.

In order to evaluate the accuracy of the algorithm developed, the mean and the standard deviation (std.) of the errors (i.e., the difference between the cardiologist annotation and our algorithm annotations) were calculated for all 105 records. To provide a means of comparison, the mean and standard deviation of the errors between the cardiologists and PhysioNet's automated annotation were also computed for the 105 records.

For further comparison, an inter-observer variability study was also carried out. This is the mean and standard deviation of the error difference between the annotations of both cardiologists in the 11 records.

Table 3.1: Summary of results for Q-onset annotations

	Num. of records	Num. of beats	Mean	Std.
Algorithm	105	3616	**-0.82 ms**	**13.4 ms**
PhysioNet	105	3619	-6.96 ms	16.5 ms

Table 3.2: Summary of results for T-offset annotations

	Num. of records	Num. of beats	Mean	Std.
Algorithm	102	3388	**-1.83 ms**	**29.82 ms**
PhysioNet	102	3309	-7.64 ms	46.48 ms

Table 3.3: Inter-observer variability study

	Q- onset			T- offset		
Records	Beats	Mean	Std.	Beats	Mean	Std.
11	404	5.24 ms	13.3 ms	401	4.94 ms	35.5 ms

The overall results of the tests are summarized in Tables 3.1, 3.2 and 3.3. Figures 3.4 and 3.5 show the distribution of the mean errors between algorithm produced anno-

tations and cardiologist annotations, and Figure 3.6 shows some algorithm annotations on three different ECG records from the QT database.

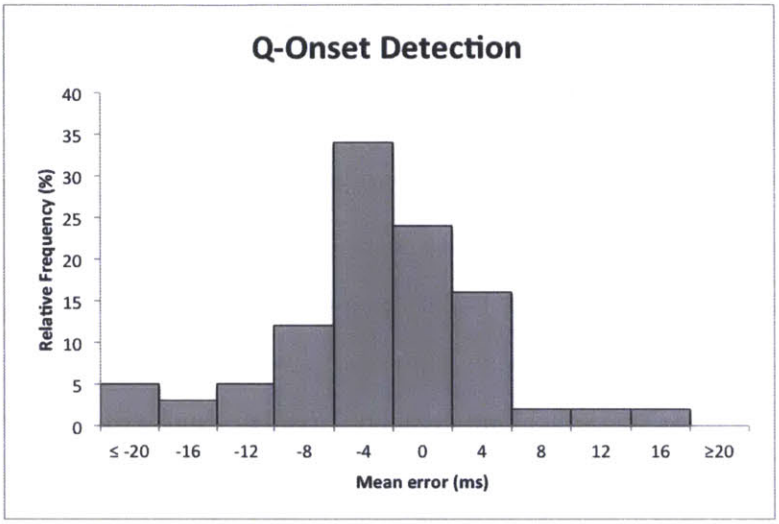

Figure 3.4: Distribution of the mean errors between algorithm produced annotations and cardiologists annotation of the Q-onset .

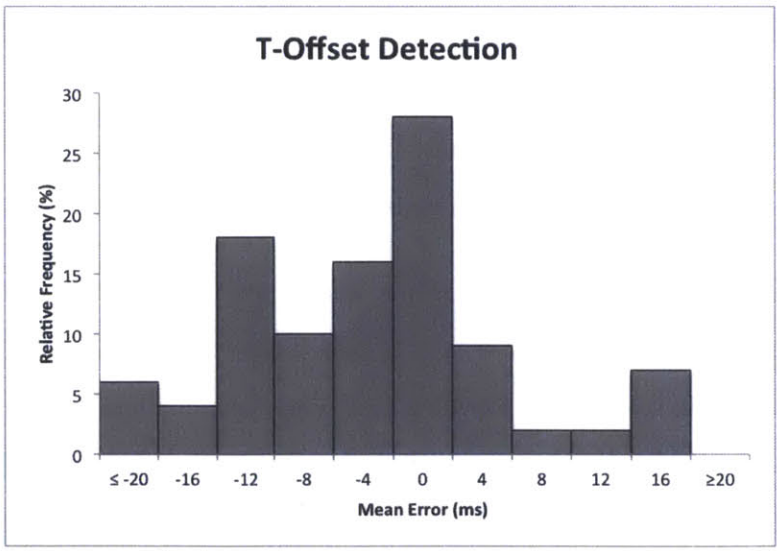

Figure 3.5: Distribution of the mean errors between algorithm produced annotations and cardiologists annotation of the T-offset .

3.4 Discussion

The inter-observer variability study show that even between experts, annotating the Q-onset and T-offset is prone to errors. It is therefore a challenge to come up with an algorithm that annotates the QT interval quite accurately. The experts had errors of 5.24 ms and 4.94 ms for the Q-onset and T-offset respectively, more than a sampling interval on average. The algorithm described in this chapter had errors of -0.82 ms and -1.83 ms for the Q-onset and T-offset respectively, less than one sampling interval on average for both cases. The algorithm also performed better than the automated annotations on PhysioNet, which had errors of -6.96 ms and -7.64 ms for the Q-onset and T-offset respectively, more than one sampling interval on average. The results show that the CLT-based algorithm detects the Q-onset and T-offset with very good accuracy.

Although the Q-onset has a low mean error, the standard deviation is about 13.4 ms, slightly more than 3 sampling intervals. This was partly due to some records that had difficult morphologies. Again, however, this is essentially the same as the standard deviation between two cardiologists.

There are some other sources of errors and potential areas for improvement. In the case of ventricular arrhythmias, the Q-onset detection would work better if the window length of 130 ms was not fixed but was predetermined based on the morphology of the QRS complexes of each record. Records that had anomalous QRS complexes characterized by a wider duration had higher Q-onset detection errors. Another source of higher errors was the use of fixed thresholding in this implementation of the algorithm. The threshold was predetermined as $1.5\times$ the mean of the CLT. This posed a problem for records that occasionally had large (and abnormal) T-waves. The part of the CLT that corresponded to these T-waves, crossed the threshold and led to a false annotation

of a QRS complex. Adaptive thresholding would allow for better performance in this case. Also records that had P-waves abnormally close to the QRS complex created problems for the algorithm. The CLT of these records was atypical and made searching for the Q-onset less reliable.

The T-offset detection relies on accurately detected Q-onsets. However, the maximum distance search process helped reduce the effect of the Q-onset errors, as long as the closing of the P-QRS portion did not affect the end of the T-wave. In addition to erroneously detected Q-onsets, tachycardic records (short RR intervals, or rapid heart rates) also contributed to large errors in the T-wave end detection. The predefined P-QRS portion can affect the T-wave end if the the RR interval is not long enough. Having an algorithm that would adjust the 160 ms interval used in the closing of the P-QRS portion, depending on the heart rate of the record, would improve detection and reduce errors.

In the chapters that follow, this algorithm is used to detect the Q-onset and T-offset, and thereby characterize of QT variability in the frequency and time domain.

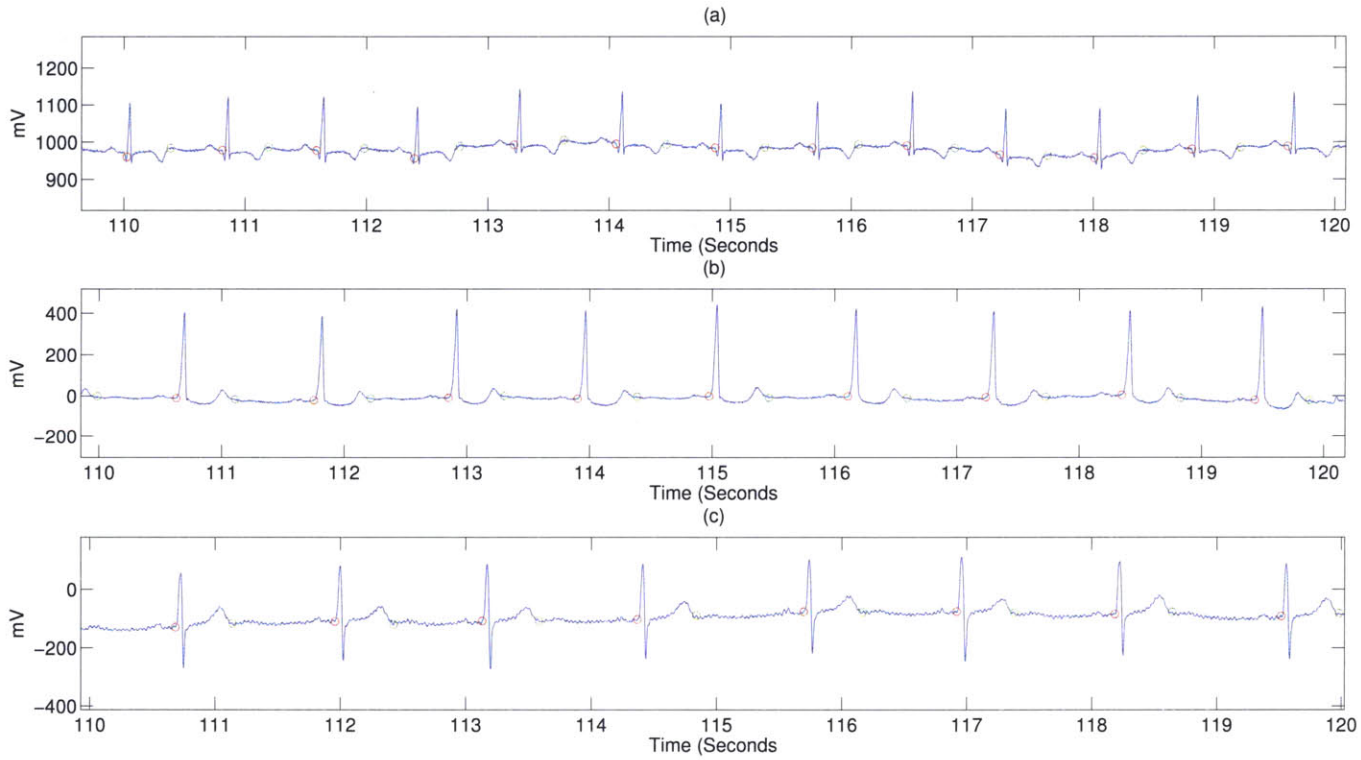

Figure 3.6: (a) ECG with inverted T-wave morphology showing algorithm's annotation of QT interval. (b) ECG showing algorithm's annotation of duration of QT interval. (c) ECG showing algorithm's annotation of QT interval.

Chapter 4

QT Variability: Spectral Methods

SPECTRAL analysis provides an estimate of the strength of different frequent components in time-domain signals. This chapter will explore the following spectral methods: power spectral density (PSD), coherence and error spectrum.

■ 4.1 QT Power Spectral Density

Power spectral density (PSD) analysis provides the basic information of how power (or the variance) in a stationary stochastic signal distributes as a function of frequency. Independent of the method employed, only an estimate of the true PSD of the signals can be obtained by proper mathematical algorithms.

After feature detection from the ECG, a time series of the QT intervals is obtained. The series obtained is non-uniformly spaced in time as a result of the inherent variability of the QT intervals. To analyze the power spectra of any series using the discrete Fourier transform (DFT), the time series needs to have uniformly spaced intervals. Resampling of the QT intervals series at a uniform rate of 2 Hz and lowpass filtering with a 1 Hz cutoff is carried out using the algorithm described by Berger *et al.* [7]. Figure 4.1 shows a time sequence of the resulting filtered QT intervals for a particular case.

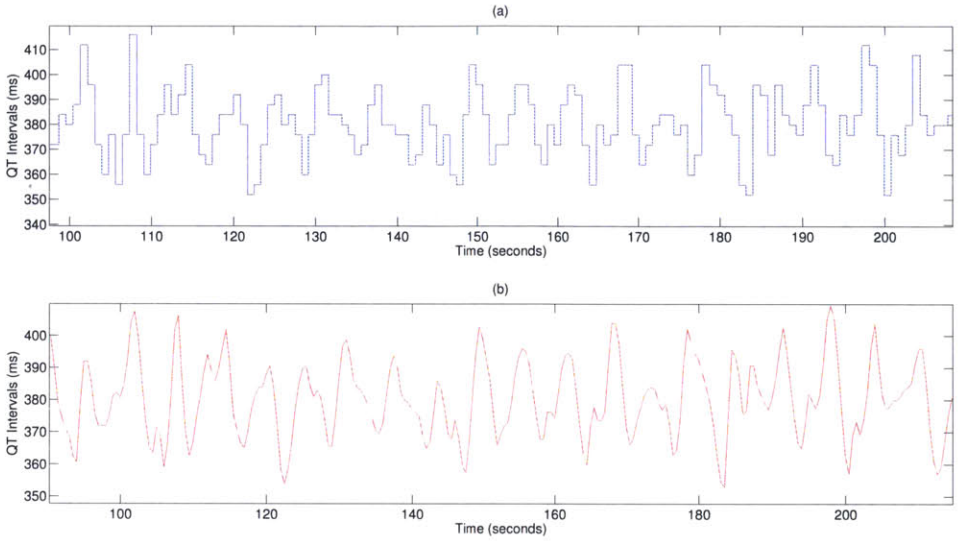

Figure 4.1: (a) Time sequence of QT intervals obtained from normal sinus rhythm (NSR) record Sel103 from the Physionet QT database [12]. (b)Uniformly sampled QT interval time series sampled at 2 *sample/s* and according the algorithm described in Berger *et al.* [7].

The method of PSD estimation employed in this thesis is called Welch's method, also known as averaged modified periodogram. The use of the fast Fourier transform (FFT) in this method allows for faster computation time and a reduction in computations needed. It consists of overlapped sectioning and windowing the data and then averaging the periodograms of the sections. Mathematically, the Fourier transform of a windowed segment of $x[n], x_r[n]$ is defined as

$$X_r(e^{j\omega}) = FT\{x_r[n]\} \tag{4.1}$$

$$= \sum_{n=0}^{L-1} w[n]x[n]e^{-j\omega n}, \tag{4.2}$$

where $w[n]$ is the window used and L is the finite number of samples in the window.

The modified periodogram estimate, $I_r(\omega)$, of this rth segment is defined as

$$I_r(\omega) = \frac{1}{LU}|V_r(e^{j\omega})|^2, \tag{4.3}$$

where U is a required normalization to remove bias. Periodogram averaging consists of time averaging K modified periodogram estimates $I_r(\omega)$ as follows

$$\overline{I}(\omega) = \frac{1}{K}\sum_{r=0}^{K-1} I_r(\omega). \tag{4.4}$$

This averaged periodogram $\overline{I}(\omega)$, estimates the PSD of the signal $x[n]$. Welch [35] showed that using a window other than the rectangular window and overlapping segments (optimum at 50% overlap), the variance of the estimate $I_r(\omega)$ reduces and it becomes a closer approximation of the actual PSD of the signal.

In the short term recording of the QT interval time series (2 *to* 5 *minutes*), there are three main frequency bands identified in its PSD estimate: very low frequency (VLF) below 0.04 Hz, low frequency (LF) from 0.04 to 0.15 Hz, and high frequency (HF) from 0.15 to 0.4 Hz. The power in the LF and HF frequency bands and the center frequency are not fixed. They vary depending on changes in autonomic control, respiration and heart period. The power in each frequency band is calculated as the area under the PSD curve between the upper and lower bounds of the bands defined above. The power in the low frequency (LFP) and high frequency (HFP) is typically expressed in normalized units (n.u.) as follows:

$$LFP(n.u) = \frac{LFP}{TP - VLFP} \tag{4.5}$$

$$HFP(n.u.) = \frac{HFP}{TP - VLFP}, \tag{4.6}$$

where VLFP is the power in the VLF band and TP is the total power from $0 - 0.4\ Hz$.

This expression in n.u., emphasizes the behavior of the SNS in the LF and PNS in the HF and reduces the effect of changes in total power on the LF and HF bands. Another measure, LF/HF, the ratio of power in the LF and HF bands, is also used as a quantitative marker of sympathovagal balance. Figure 4.2 shows a two sided QT PSD of a normal sinus rhythm patient with a LF, HF and HF harmonics peak in the high frequency band.

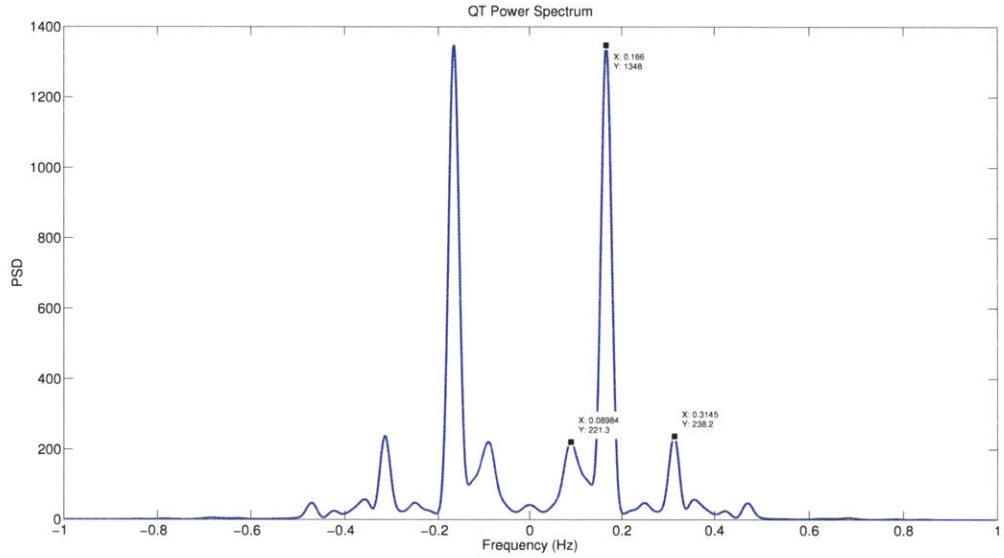

Figure 4.2: Two-sided power spectrum of QT intervals of five minutes of normal sinus rhythm (NSR) record Sel103 (from PhysioNet QT database [12]), showing a LF peak at 0.09 Hz, a strong HF peak 0.16 Hz, and another peak at 0.314 Hz, possibly a harmonic of the HF peak.

■ 4.2 Linear Prediction of QT from RR Interval

The QT interval is embedded in the RR interval, and this brings up the issue of how much of QT interval variability is driven by RR interval variability. This has led to the study of QT-RR coupling strength. The less the RR interval can predict the QT interval, the less coupled the QT and RR intervals are, and the more independent QT

variability is from RR variability. The major spectral method used to study the QT-RR coupling strength is spectral coherence. This has as interesting interpretation in the setting of linear prediction [6], though this has not been built on in the literature. We also propose a new spectral method to quantify QT variability independent of RR variability: residual error spectrum.

■ 4.2.1 Coherence

The coherence between QT and RR intervals measures how well the QT interval can be estimated or predicted from the RR intervals by passing the RR intervals through an optimum (and generally non-causal) linear time-invariant (LTI) filter, also known as the Wiener filter. The QT and RR interval series are uniformly sampled according to the algorithm described in Berger *et al* [7], and the power spectra, P_{xx} and P_{yy}, of the RR and QT time series respectively, as well as their cross spectrum, P_{xy}, are computed. The coherence function is computed according to the following relation:

$$\gamma(f) = |\rho|^2 = \frac{|P_{xy}(f)|^2}{P_{xx}(f)P_{yy}(f)}, \qquad 0 \leq \gamma(f) \leq 1, \tag{4.7}$$

where ρ is the frequency-domain correlation coefficient. From the the equation above, it can be seen that the effects of very low power in higher frequencies of P_{xx} or P_{yy} will cause the coherence to be quite noisy. As a result, a correction term δ is added to the equation as follows:

$$\hat{\gamma}(f) = \frac{|P_{xy}(f)|^2}{(P_{xx}(f) + \delta_x)(P_{yy}(f) + \delta_y)}, \qquad 0 \leq \gamma(f) \leq 1 \tag{4.8}$$

The correction term δ, is chosen as the highest PSD value in the frequency region where we are not concerned about the power content, i.e., the region of $0.4 - 1Hz$. Although

this introduces an error to the correlation function $\gamma(f)$, if δ is chosen small enough, the frequency areas with very strong correlation (areas we are interested in) are not significantly affected.

The higher the coherence, the more coupled the QT interval is to the RR interval, in the sense that one series can be well approximated (in a mean-square error sense) by linear, time-invariant (LTI) filtering of the other. One issue with this index is that the LTI filter associated with this estimation is non-causal. The coherence function cannot be used to infer causality and does not allow the predefinition of the direction of the interactions between the QT and RR intervals. For illustrative purposes, Figure 4.3 shows a plot of the PSD of RR and QT intervals superimposed. Figure 4.4 shows the corrected coherence function from Eq. (4.8), with strong peaks corresponding to areas of high coherence, or frequency regions where the RR interval can predict the QT interval within a reasonable level of accuracy.

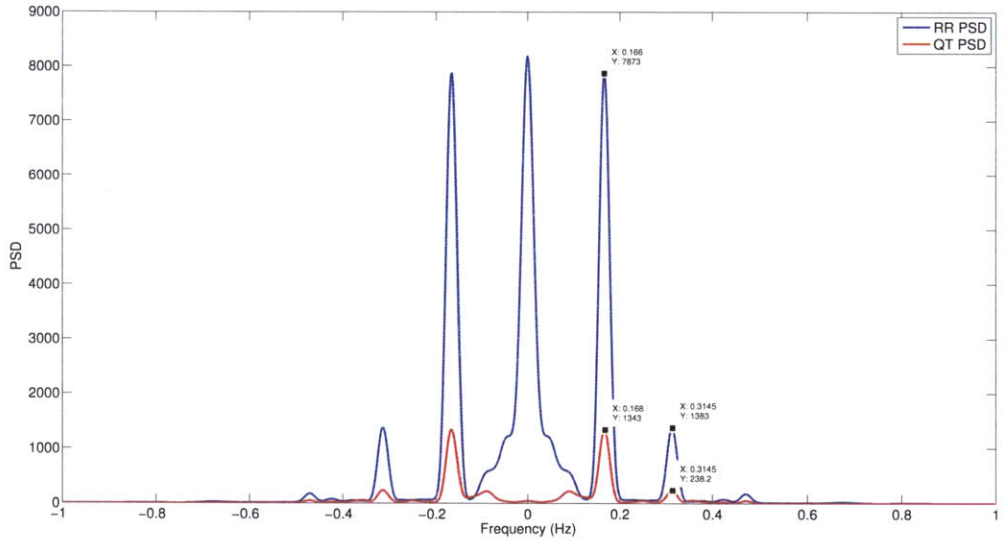

Figure 4.3: RR and QT intervals two-sided PSD of five minutes of normal sinus rhythm (NSR) record Sel103 (from PhysioNet QT database [12]), showing similar peaks at 0.166 Hz and another at 0.314 Hz.

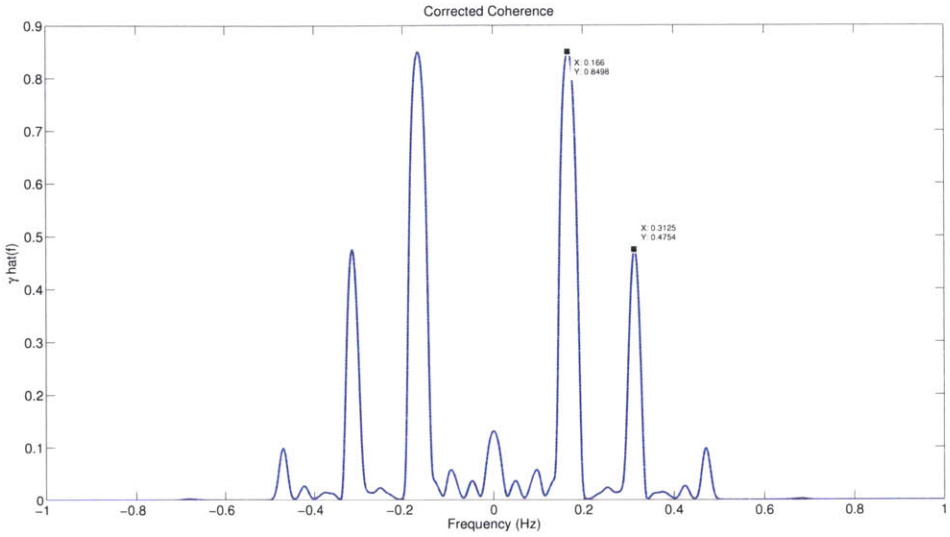

Figure 4.4: Corrected coherence of QT and RR intervals (spectra shown in Figure 4.3), showing a strong correlation of about 0.9 at 0.166 Hz and another of about 0.5 at 0.314 Hz (possibly as a result of the presence of a harmonic).

■ 4.2.2 Residual Error Power

Although the non-causal Wiener prediction of the QT interval $\hat{QT}$ from the RR interval is optimum in the minimum mean squared error sense, it produces a residual error, e, defined as

$$e = QT - \hat{QT} \tag{4.9}$$

It can be said that this error comprises of the part of the QT interval that cannot be linearly predicted from the RR interval. Thus, the residual error contributes to the part of QT variability that is not influenced by RR variability. Another quantitative method of characterizing QT variability independent of RR variability (especially in normal sinus rhythm cases), is by computing the PSD of the residual error.

Dropping the frequency argument for notational convenience, the PSD of the error, P_{ee}, is defined as

$$P_{ee} = P_{yy} - HPxy, \tag{4.10}$$

where H is the transfer function of the non-causal Wiener filter and is defined as

$$H = \frac{P_{yx}}{P_{xx}}. \tag{4.11}$$

The residual error spectrum now becomes

$$\begin{aligned} P_{ee} &= P_{yy} - \frac{P_{yx}}{P_{xx}} Pxy && (4.12)\\ &= P_{yy}(1 - \frac{P_{yx}}{P_{yy}P_{xx}} Pxy) && (4.13)\\ &= P_{yy}(1 - \frac{|P_{xy}|^2}{P_{yy}P_{xx}}) && (4.14)\\ &= P_{yy}(1 - |\rho|^2) && (4.15) \end{aligned}$$

The equation above shows that the residual error spectrum is indeed what is left after the QT interval has been linearly predicted from the RR interval. The power in the error is calculated as the area under the curve of the P_{ee} within the frequency bands of interest.

Figure 4.5 shows the spectrum of the residual error. The influence of the dominant frequency peak in the RR spectrum is removed and the LF peak that cannot be predicted by the RR interval is dominant.

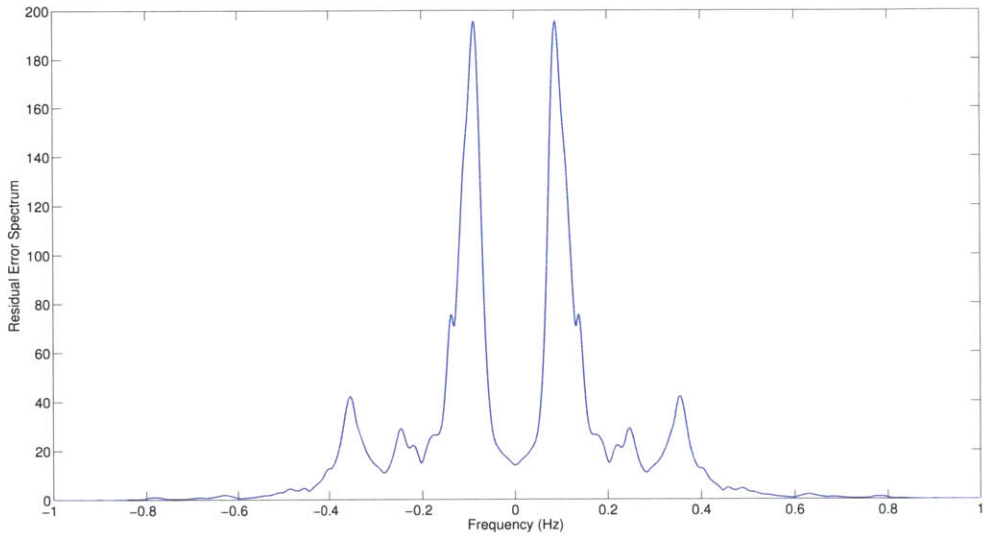

Figure 4.5: Power spectrum of residual error showing dominant peak at 0.09 Hz. The breathing frequency peak at 0.166 Hz contributes very little to the power.

Chapter 5

QT Variability: Tilt Table Data

THE graded head-up tilt experiment imposes a progressive increase in the activity and modulation of the sympathetic nervous system (SNS)[30]. Since QT intervals are primarily influenced by the activation of the SNS, quantifying the variability of the QT intervals obtained from this experiment would provide a quantitative assessment of SNS activity on the heart.

5.1 Methods

ECGs were obtained from ten healthy subjects undergoing the tilt table experiment. Each subject was placed on a tilt table with foot support, and underwent a series of six postural changes: two stand-ups, two rapid tilts and two slow tilts. The sequence of intervention was randomized for each subject. More details are explained in Heldt *et al.* [14].

Our QT detection algorithm was used to annotate the Q-onsets and T-offsets of the ECG. The R peaks were detected by doing a maximum point search along the ECG interval in-between each detected Q-onset and T-offset. Figure 5.11 shows annotations of Q-onset, T-offset and R peak of a tilt table data record using the algorithm.

5.2 Results of Time Series Analysis

The QT and RR intervals obtained were plotted against time. Figures 5.1 and 5.2 show the results that were obtained from two subjects. Other results are shown in Appendix A. The red lines indicate the transition time from one intervention to a rest period. The difference in adaptation to the changes from one intervention to a rest period is quite clear. Looking at individual transitions, it is evident that the QT intervals adapted quite slowly in comparison with the quick adaptation of the RR intervals. Figures 5.3, 5.4 and 5.5 show the results from the subject's supine position before the intervention (before the red lines), the subject's upright position during the intervention (in-between the red lines), and finally the subject's supine position after the interventions, for the slow tilts, rapid tilts and stand-ups respectively. Note that in the case of the slow tilts, the first two and last two red lines indicate the duration of the slow tilt-up and slow tilt-down respectively.

The adaption of the QT interval when the subject is in a tilted position (during an intervention) and when the subject is returning to supine position (after an intervention) appears exponential. After low pass filtering the QT time series, least-squares fitting was used to fit a single exponential to the QT response characteristics. This enabled us to estimate the time constant, τ, of the autonomic activity on the QT interval, thus providing as estimate of the sympathetic time constant. The model used for the exponential fit is as follows:

$$QT = QT(t = \infty) - \Big(QT(t = \infty) - QT(t = 0)\Big) * e^{-\lambda t} \tag{5.1}$$

where $\lambda = 1/\tau$, and where $t = 0$ and $t = \infty$ denote the start and the asymptote of the adaptation transient. Taking logs converts this to a linear estimation problem (see

Appendix C). Figure 5.6 shows the fitting of an exponential to two of the QT interval transients and Table 5.1 contains the estimated time constants of subject 12755.

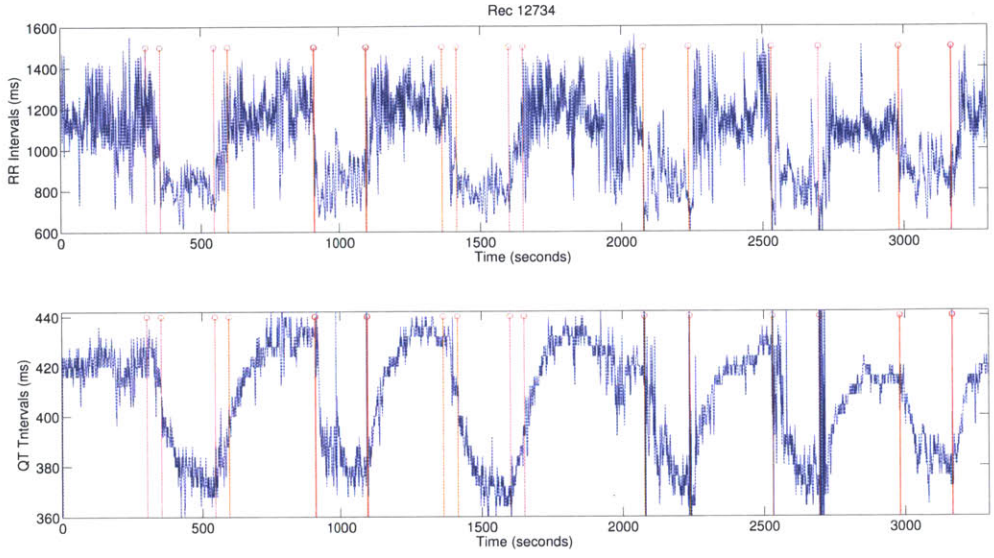

Figure 5.1: RR and QT interval time series- Subject 12734.

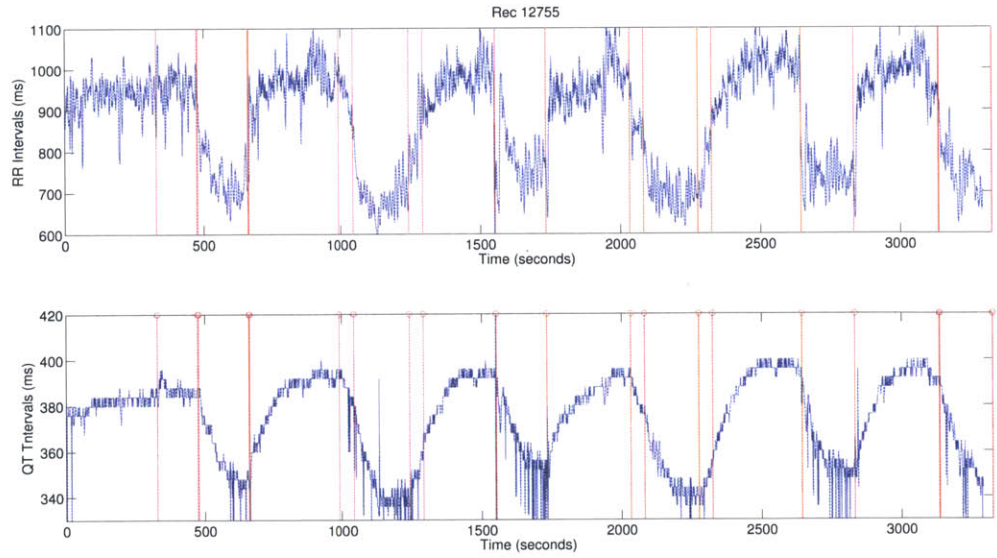

Figure 5.2: RR and QT interval time series- Subject 12755.

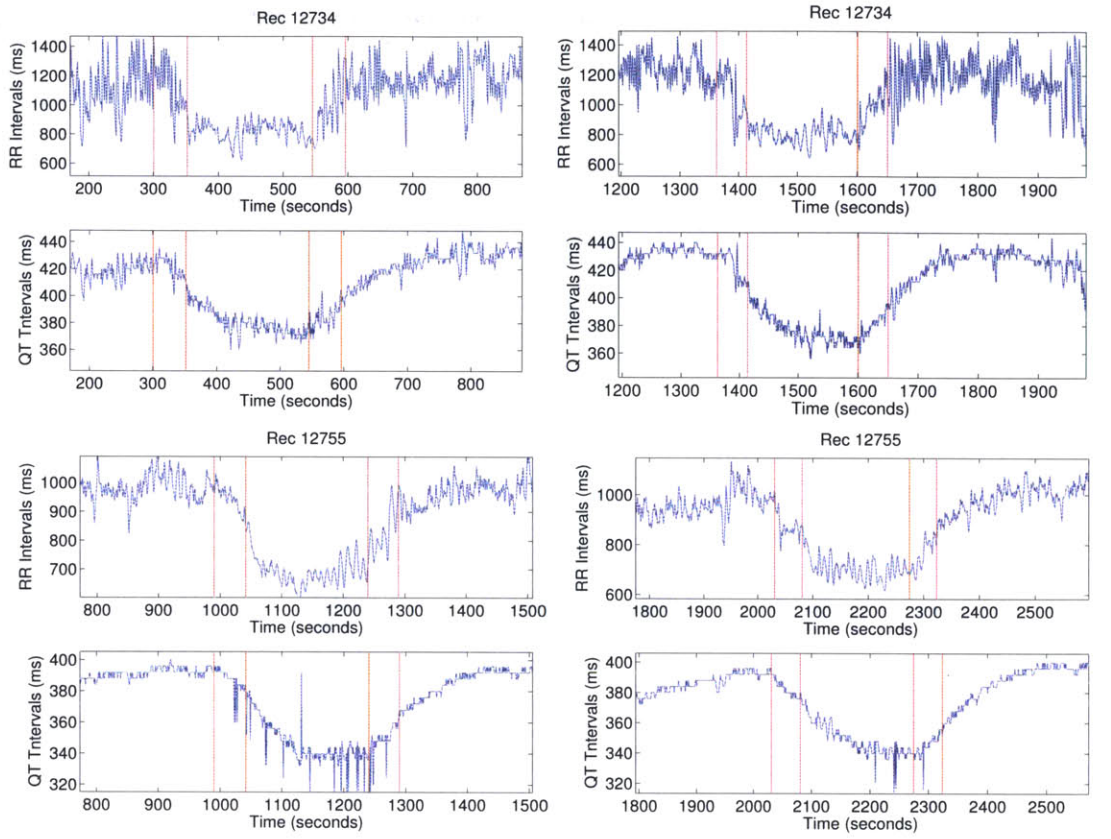

Figure 5.3: From L-R: first and second slow tilts of subject 12734 *(top)*, first and second slow tilts of subject 12755 *(bottom)*.

The SNS activity is a much slower acting system than the PNS, and thus changes in the QT interval as a result of SNS activation will produce a slower transient. The RR intervals on the other hand are primarily modulated by the parasympathetic nervous system, a much faster system; this is the reason for a much faster RR interval adaptation to changes produced by tilting the subjects.

This interesting exponential trend also gives rise to questions about the validity of normalizing QT intervals to heart rate. As mentioned in Chapter 2, QT intervals are often normalized to remove the dependence of the QT intervals on heart rate, but

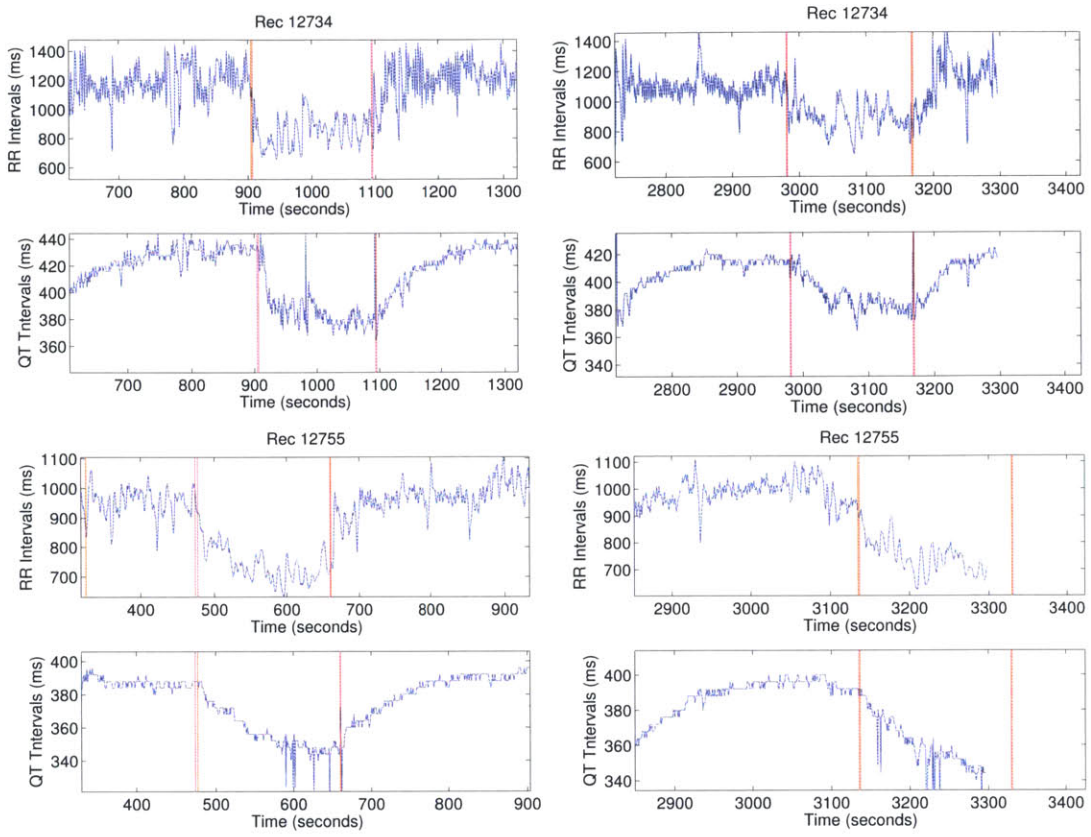

Figure 5.4: From L-R: first and second rapid tilts of subject 12734 *(top)*, first and second rapid tilts of subject 12755 *(bottom)*.

as illustrated in Figure 5.7, the corrections dampen the slow rise and fall of the QT intervals, making them less apparent.

■ 5.3 Results of Spectral Analysis

Spectral analysis of the tilt table data was also carried out on the part of the data that has attained steady state (i.e., after transients). After resampling and filtering the QT and RR interval tachogram at 2Hz using the algorithm described by Berger

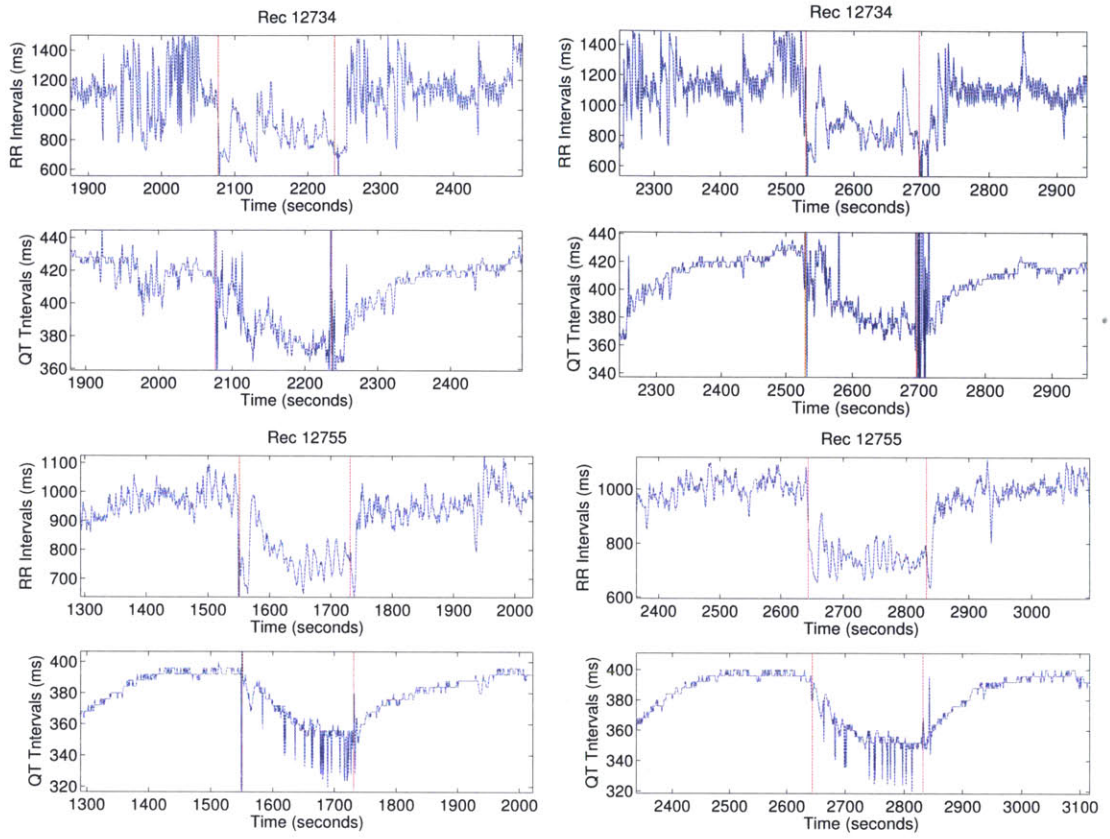

Figure 5.5: From L-R: first and second stand-ups of subject 12734 *(top)*, first and second stand-ups of subject 12755 *(bottom)*.

et al. [7], power spectra were obtained by using Welch's method. The direct current (DC) component was removed by subtracting the mean value of the data set. A sliding Hamming window of 512 points or 1024 points (depending on the length of the segment analyzed) with 50% overlap was used. As frequency domain measures, LF (n.u.), HF (n.u.) and LF/HF were calculated. Figures 5.8 and 5.9 show a PSD plot of a slow-tilt up and Figure 5.10 shows the plot of the residual error spectrum. Some other examples are in Appendix B. Tables 5.2 - 5.7 summarize the values obtained from frequency domain normalized power calculations.

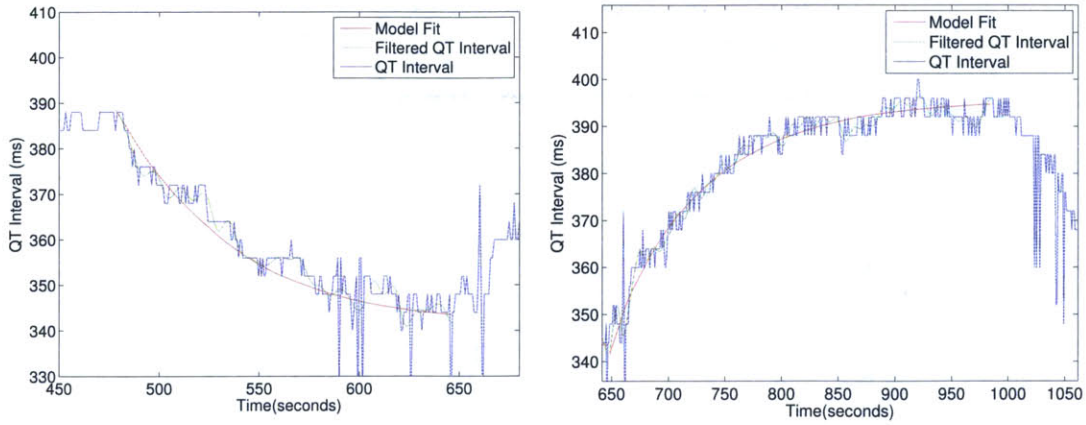

Figure 5.6: From L-R: diagram showing exponential fitting of QT adaptation after rapid tilt and the immediate resting period.

Table 5.1: Estimated time constants (τ)

	τ (sec)	Average τ (sec)
Rapid tilt	72.0	72
Slow tilts	99.0	94
	88.9	
Stand-ups	79.5	78
	76.3	
Transitions to supine	89.3	79
	81.8	
	81.9	
	69.4	
	77.6	

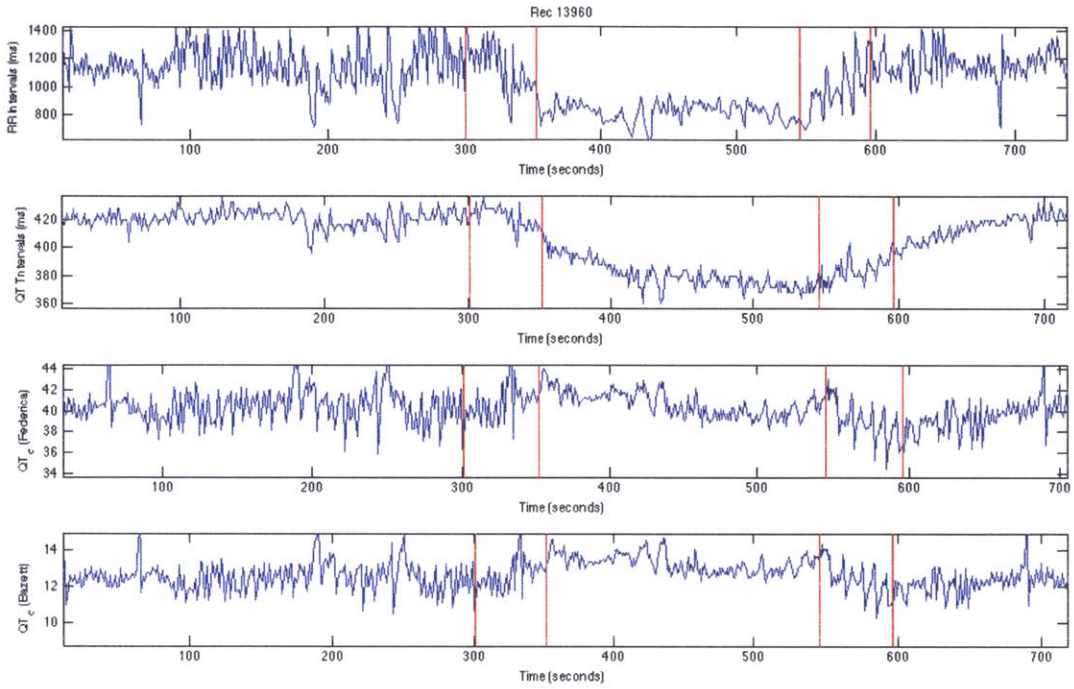

Figure 5.7: Illustration of QT normalization using intervals from subject 13960.

Table 5.2: First slow tilt-up

	Before tilt-up			After tilt-up		
	LF (n.u)	HF (n.u)	LF/HF	LF (n.u)	HF (n.u)	LF/HF
RR	0.51	0.48	1.07	0.61	0.33	1.87
QT	0.61	0.36	1.63	0.61	0.33	1.87

Table 5.3: Second slow tilt-up

	Before tilt-up			After tilt-up		
	LF (n.u)	HF (n.u)	LF/HF	LF (n.u)	HF (n.u)	LF/HF
RR	0.45	0.53	0.85	0.83	0.14	6.01
QT	0.59	0.39	1.51	0.65	0.32	2.07

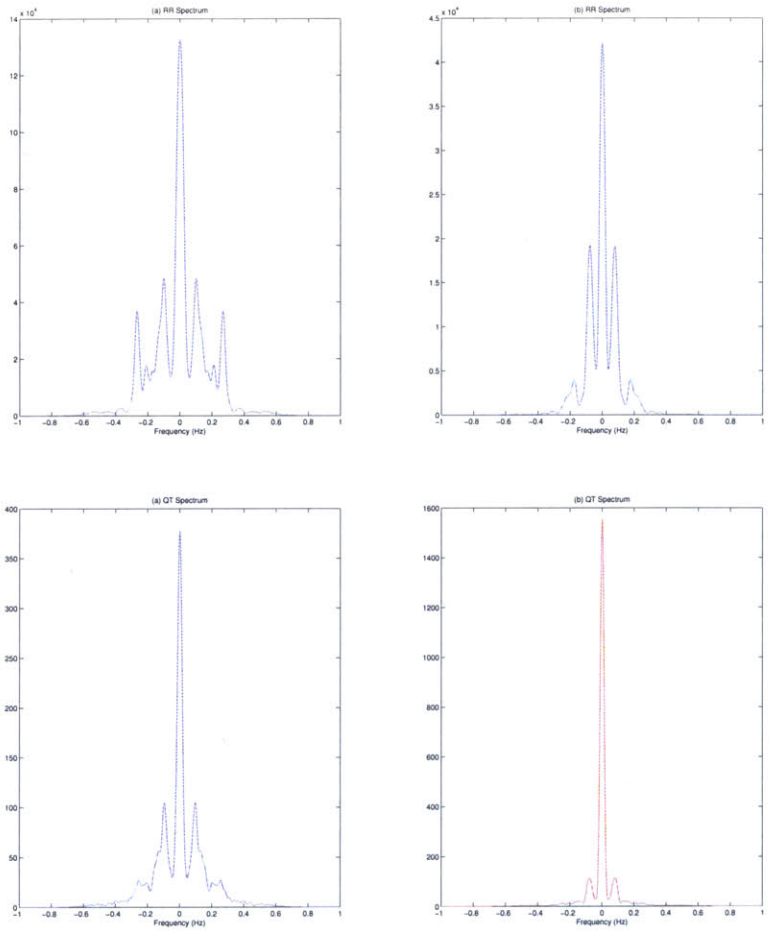

Figure 5.8: From L-R: PSD before and after first slow tilt up of 12734. Time series shown in the top plots in Figure 5.3. RR PSD *(top)* and QT PSD *(bottom)*.

Table 5.4: First rapid tilt-up

	Before tilt-up			After tilt-up		
	LF (n.u)	HF (n.u)	LF/HF	LF (n.u)	HF (n.u)	LF/HF
RR	0.62	0.35	1.79	0.83	0.13	6.26
QT	0.63	0.34	1.83	0.50	0.46	1.09

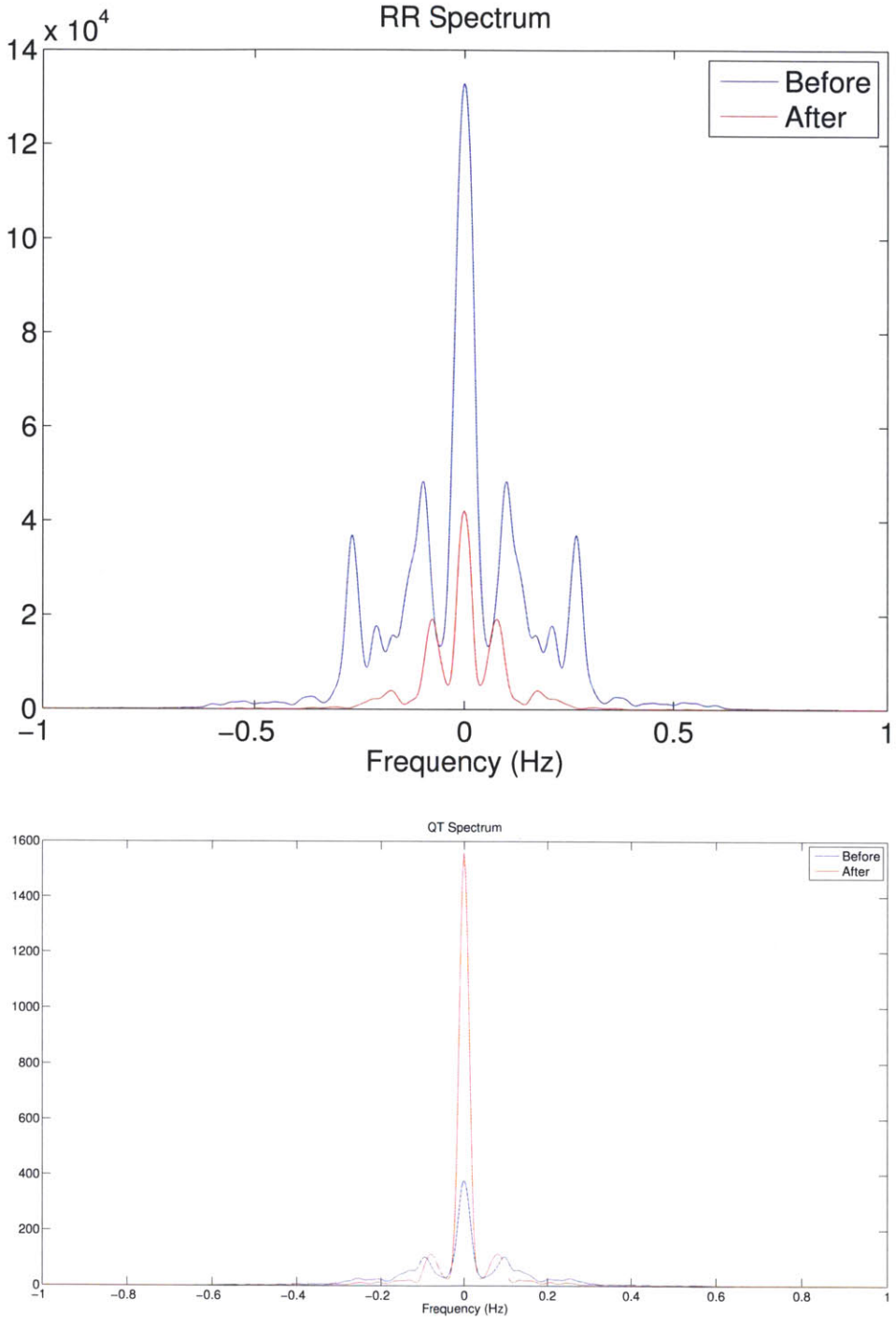

Figure 5.9: Illustration of the change in power before and after slow tilt-up

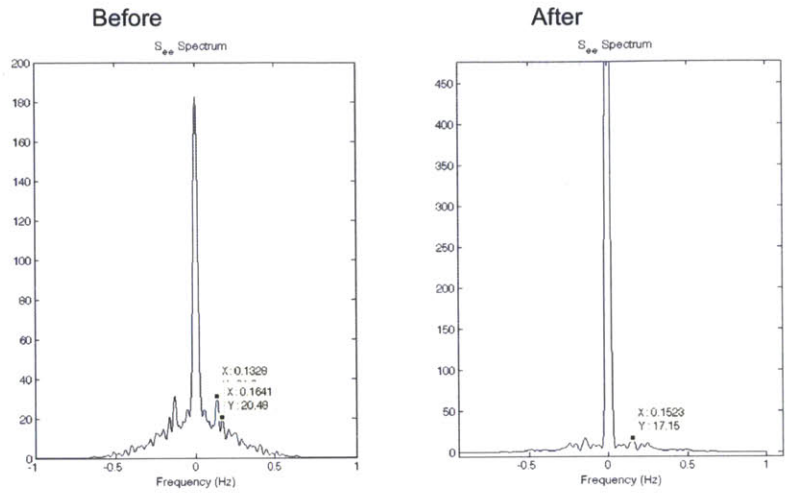

Figure 5.10: Residual error spectrum of first slow tilt-up of record 12734

Table 5.5: Second rapid tilt-up

	Before tilt-up			After tilt-up		
	LF (n.u)	HF (n.u)	LF/HF	LF (n.u)	HF (n.u)	LF/HF
RR	0.35	0.58	0.61	0.77	0.13	6.02
QT	0.50	0.41	1.22	0.67	0.22	3.05

Table 5.6: First stand-up from supine

	Supine			Stand-up		
	LF (n.u)	HF (n.u)	LF/HF	LF (n.u)	HF (n.u)	LF/HF
RR	0.50	0.44	1.15	0.72	0.18	3.83
QT	0.64	0.30	2.13	0.54	0.38	1.41

Table 5.7: Second stand-up from supine

	Supine			Stand-up		
	LF (n.u)	HF (n.u)	LF/HF	LF (n.u)	HF (n.u)	LF/HF
RR	0.39	0.59	0.66	0.68	0.18	3.82
QT	0.50	0.45	1.13	0.50	0.43	1.18

From the results in tables 5.2-5.6, the LF peak and normalized power of the QT spectra do not change much before and after the interventions. In the case of the RR spectra, there is a dramatic increase in LF normalized power and a more prominent LF peak during the interventions that stimulate an activation of the sympathetic nervous system, i.e., tilted positions and the stand up posture. The slower oscillations that are seen in the RR intervals during the activation of the SNS contributes to the increase of the LF normalized power. The stability of the QT spectra before and after interventions shows that the QT is primarily affected by the SNS.

High frequency components of the QT spectra are not dominant. This signifies lower dependence of the QT interval on PNS activity. This is in direct contrast with the spectrum of the RR intervals. In RR spectra, the HF components significantly reduce when the SNS is activated, implying a reliance of the RR interval on the PNS. This reduction in HF power also establishes the fact that the activation of the SNS is accompanied by inhibition of the activity of the PNS and vice versa.

The LF/HF ratio of the RR intervals increases drastically when the SNS is activated. This is as a result of a shift in the sympathovagal balance: from parasympathetic dominance to sympathetic dominance. This shift is not quite represented in the LF/HF ratio of the QT spectra. Also, the power of the residual error spectra is barely changed, implying that RR variability does not contribute a lot to QT variability before and af-

ter interventions. This is in agreement with fact that in an experiment where the SNS activity is highlighted, its primary modulation of the QT interval in also highlighted. Thus, it shows that QT variability is driven primarily by the modulation of the SNS.

In general, RR intervals shows a significant decrease in total spectral power when the SNS is activated, and consequently PNS is withdrawn, while QT has a LF peak that remains quite constant all through the experiment. This demonstrates, through the frequency domain, that QT intervals are primarily affected by SNS and RR intervals are primarily affected by PNS.

In summary, the results in both frequency and time domain demonstrate a clear difference between the response of the QT intervals and of the RR intervals to the SNS. The characteristics of the SNS such as slow response time and dominant LF activity are highlighted by looking at the variability of the QT intervals. This has shown that QT variability indeed has potential to be a quantitative marker of sympathetic nervous system modulation.

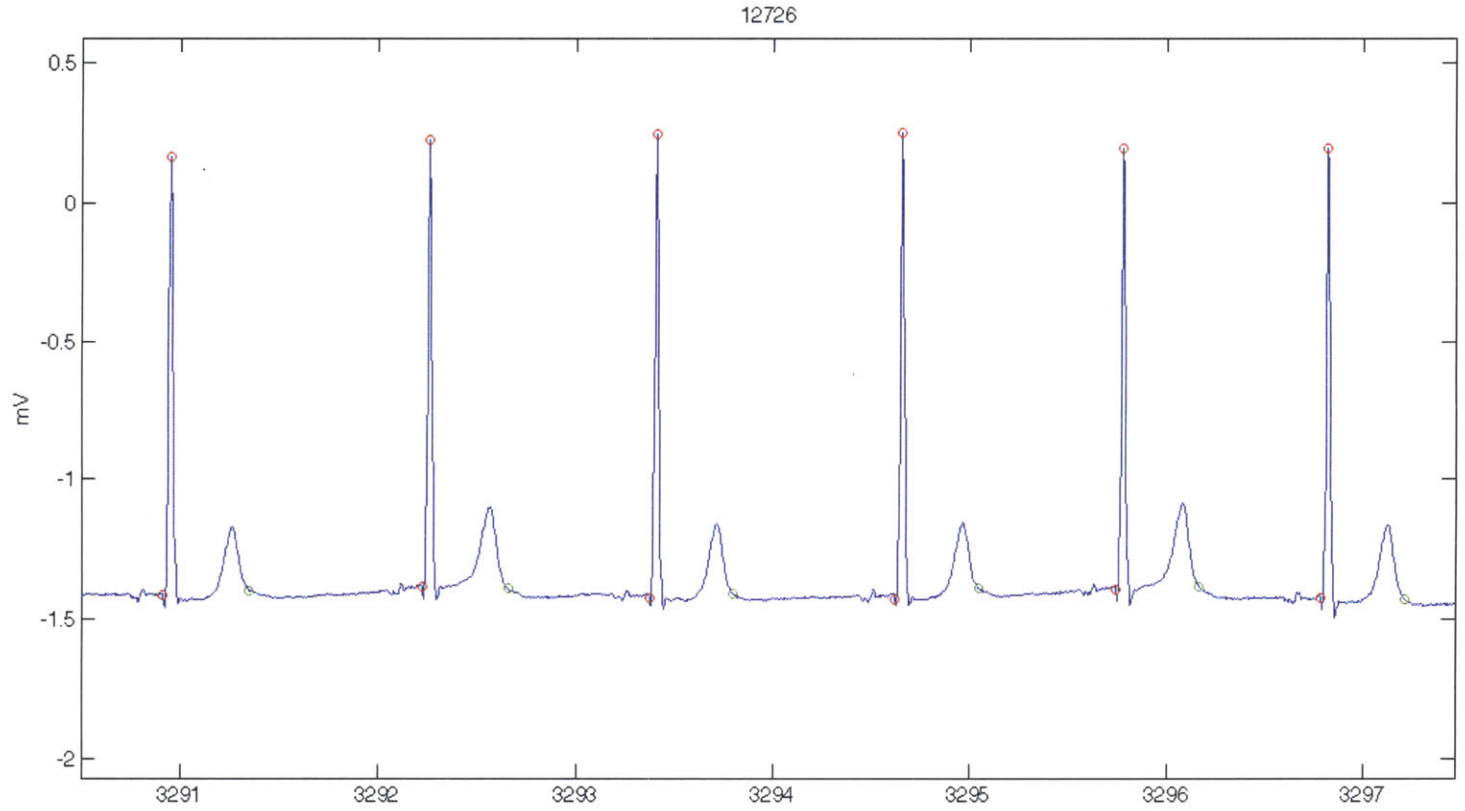

Figure 5.11: Annotation of an ECG from tilt table data.

Chapter 6

Conclusion

THE strong role of the autonomic nervous system in cardiovascular activities has been long established. While heart rate variability has been the well established means of assessment, QT variability has now proved to be a potential quantitative marker of cardiac autonomic tone effected through the sympathetic nervous system.

The fact that the QT interval is embedded in the RR interval gives rise to a need for independent variability characterization. The residual error spectrum was proposed as a new way of quantifying QT variability independent of RR variability. The use of spectral coherence as it relates to both the QT and RR intervals was also re-defined, with the coherence being used as an indicator of how well the RR intervals can linearly predict the QT intervals. This is also an indication of how independent QT variability is from RR variability.

The time-domain analysis showed a striking difference between the way QT and RR intervals adapt to changes in autonomic balance. The fast response of the RR intervals imply that they are primarily modulated by the parasympathetic nervous system, while the slow response of the QT intervals indicate that that they are primarily modulated by the sympathetic nervous system. Since the QT intervals and RR intervals are modulated primarily by the different branches of the autonomic nervous system, it is necessary to

always take both QT and RR variability into account when assessing cardiac autonomic tone.

Although it is clear that QT variability is the primary maker of sympathetic nervous system activity in the heart, more work still needs to be done in order to develop algorithms that can accurately quantify its modulation via QT variability.

Another future goal is the adaptation of non-linear methods in the assessment of QT-RR coupling. The relationship between QT and RR intervals is non-linear and so in order to fully characterize the interaction between the cardiovascular system and the autonomic nervous system, a combined linear and non-linear approach is needed. In addition to existing methods, conditional entropy can also make it possible to explore the coupling of the QT and RR intervals non-linearly, and to also develop a quantitative marker of sympathetic activity via QT variability.

The availability of linear and non-linear algorithms for QT variability assessment will be useful in the detection of ventricular abnormalities in the early stages of brain injury or other impaired ventricular regulation.

Appendix A

Tilt Table Data Results

A.1 RR, QT Intervals

The plots below show a time plot of the RR intervals on the top, and QT intervals on the bottom. The red lines dividing each plot mark the initiation and conclusion of each of the interventions performed. The list of annotations indicates (in order of left to right) which intervention is marked by each of the red lines.

1. Record 12726

Annotations for Figure A.1

1. Initiate slow tilt up
2. Conclude slow tilt up
3. Initiate slow tilt down
4. Conclude slow tilt down
5. Initiate and conclude rapid tilt up
6. Movement artifacts
7. Initiate and conclude rapid tilt down
8. Stand up and lost ECG signal due to poor electrode-skin contact
9. Transition back to supine

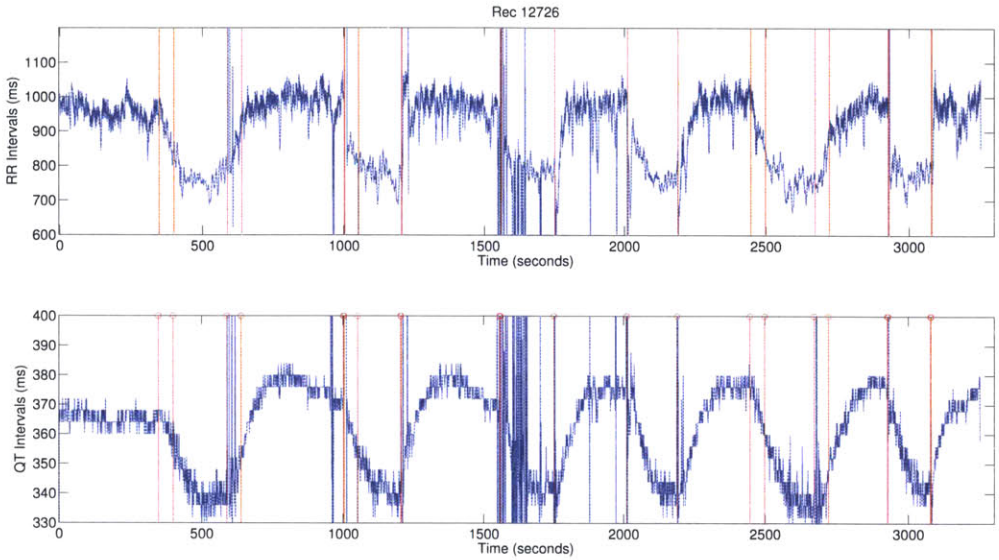

Figure A.1: 12726

10. Stand up
11. Transition back to supine
12. Initiate slow tilt up
13. Conclude slow tilt up
14. Initiate slow tilt down
15. Conclude slow tilt down
16. Initiate and conclude rapid tilt up
17. Initiate and conclude rapid tilt down

2. Record 12734

Annotations for Figure A.2

1. Initiate slow tilt up
2. Conclude slow tilt up
3. Initiate slow tilt down

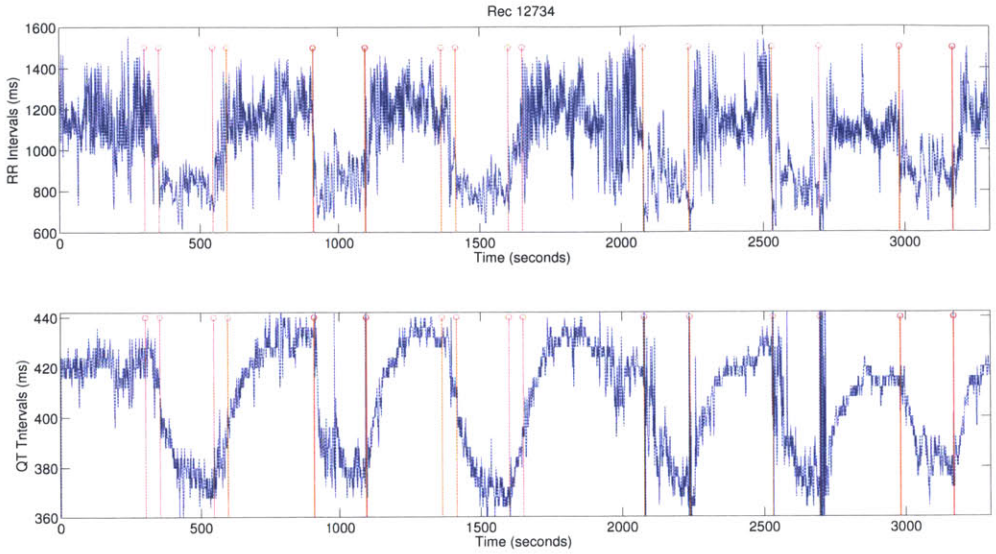

Figure A.2: 12734

4. Conclude slow tilt down
5. Initiate and conclude rapid tilt up
6. Initiate and conclude rapid tilt down
7. Initiate slow tilt up
8. Conclude slow tilt up
9. Initiate slow tilt down
10. Conclude slow tilt down
11. Stand up
12. Transition back to supine
13. Stand up
14. Transition back to supine
15. Initiate and conclude rapid tilt up
16. Initiate and conclude rapid tilt down

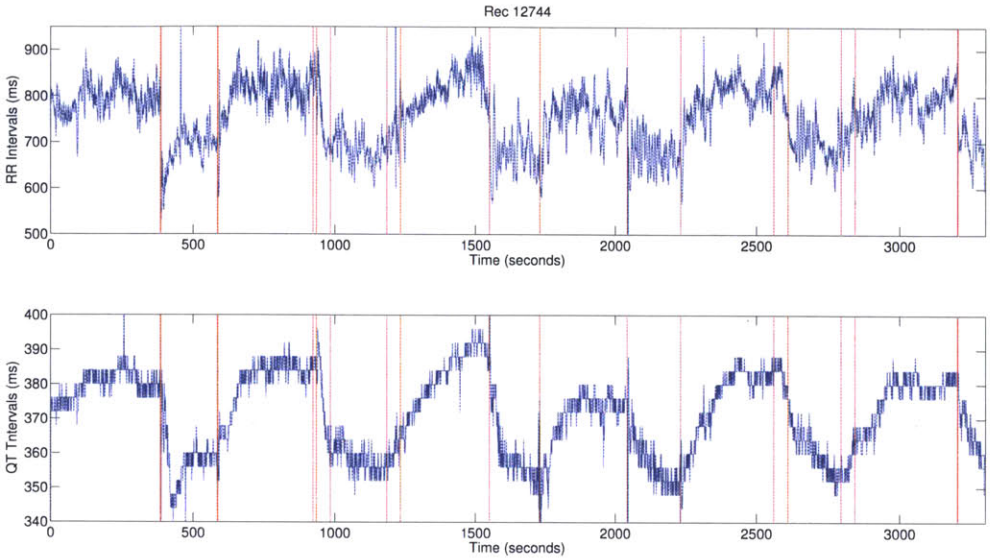

Figure A.3: 12744

3. Record 12744

Annotations for Figure A.3

1. Initiate and conclude rapid tilt up
2. Initiate and conclude rapid tilt down
3. Misfire of marker signal
4. Initiate slow tilt up
5. Conclude slow tilt up
6. Initiate slow tilt down
7. Conclude slow tilt down
8. Stand up
9. Transition back to supine
10. Stand up
11. Transition back to supine

12. Initiate slow tilt up
13. Conclude slow tilt up
14. Initiate slow tilt down
15. Conclude slow tilt down
16. Initiate and conclude rapid tilt up

4. Record 12754

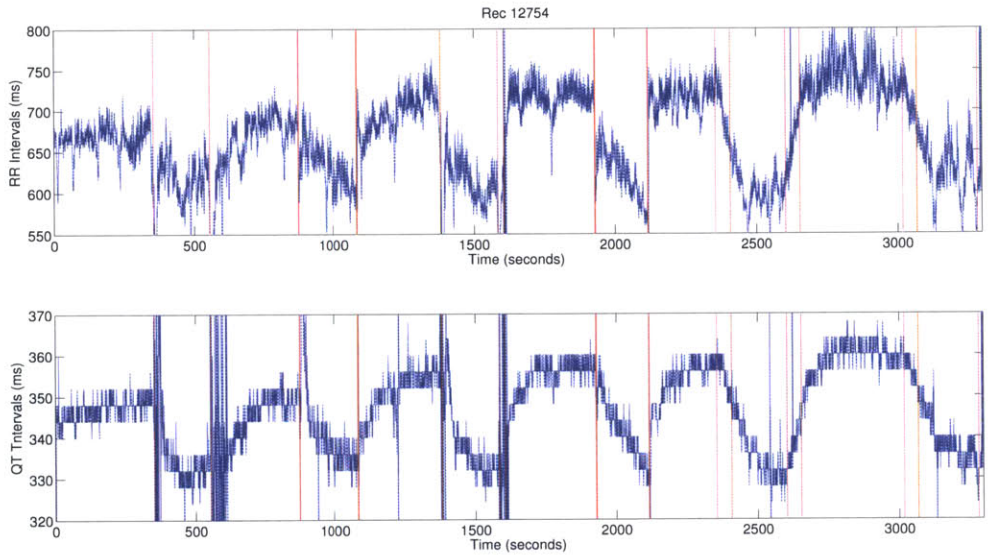

Figure A.4: 12754

Annotations for Figure A.4

1. Stand up
2. Transition back to supine
3. Initiate and conclude rapid tilt up
4. Initiate and conclude rapid tilt down
5. Stand up

6. Transition back to supine
7. ECG noise due to poor electrode contact
8. Initiate and conclude rapid tilt up
9. Initiate and conclude rapid tilt down
10. Initiate slow tilt up
11. Conclude slow tilt up
12. Initiate slow tilt down
13. Conclude slow tilt down
14. Initiate slow tilt up
15. Conclude slow tilt up
16. Initiate slow tilt down

5. Record 12755

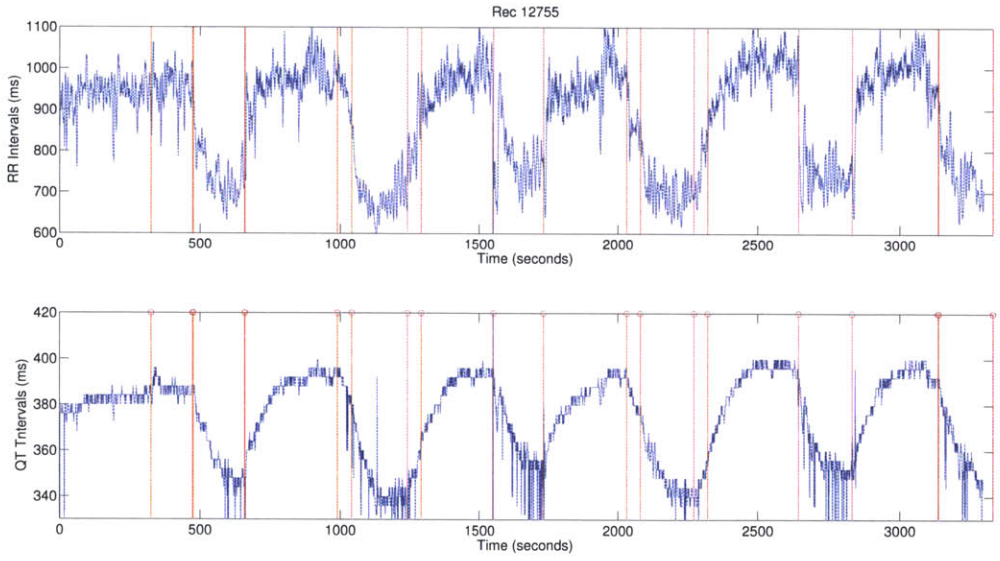

Figure A.5: 12755

Annotations for Figure A.5

1. Failed attempt to tilt rapidly
2. Initiate and conclude rapid tilt up
3. Initiate and conclude rapid tilt down
4. Initiate slow tilt up
5. Conclude slow tilt up
6. Initiate slow tilt down
7. Conclude slow tilt down
8. Stand up
9. Transition back to supine
10. Initiate slow tilt up
11. Conclude slow tilt up
12. Initiate slow tilt down
13. Conclude slow tilt down
14. Stand up
15. Transition back to supine
16. Initiate and conclude rapid tilt up
17. Initiate and conclude rapid tilt down

6. Record 12815

Annotations for Figure A.6

1. Initiate slow tilt up
2. Conclude slow tilt up
3. Initiate slow tilt down
4. Conclude slow tilt down
5. Initiate and conclude rapid tilt up

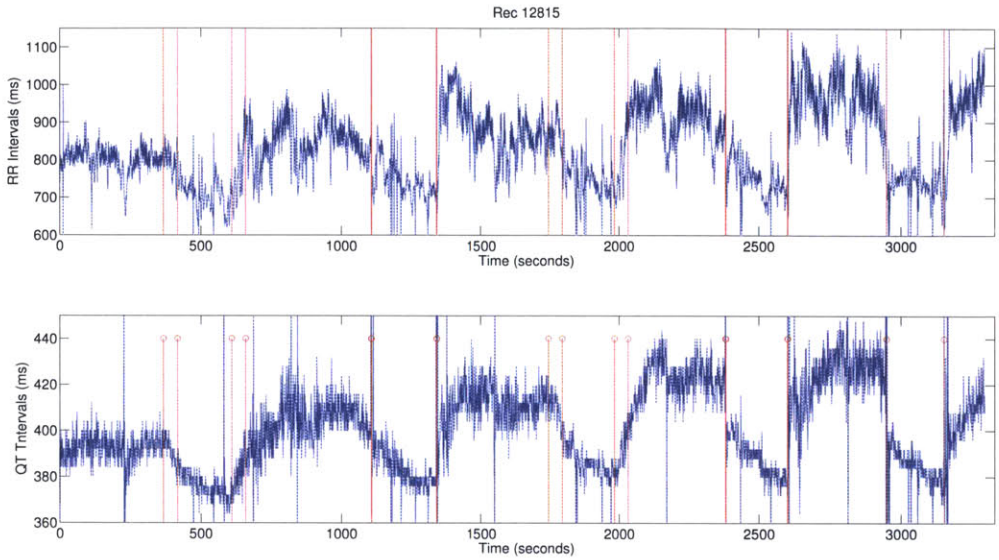

Figure A.6: 12815

6. Initiate and conclude rapid tilt down
7. Initiate slow tilt up
8. Conclude slow tilt up
9. Initiate slow tilt down
10. Conclude slow tilt down
11. Initiate and conclude rapid tilt up
12. Initiate and conclude rapid tilt down
13. Stand up
14. Transition back to supine
15. Stand up
16. Transition back to supine

7. Record 12819

Annotations for Figure A.7

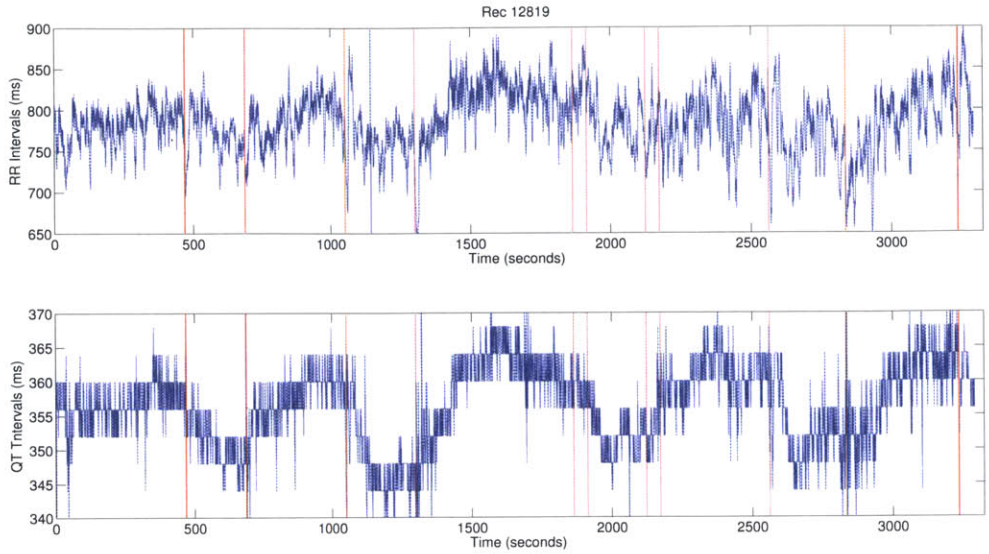

Figure A.7: 12819

1. Initiate and conclude rapid tilt up
2. Initiate and conclude rapid tilt down
3. Stand up
4. Transition back to supine
5. Initiate slow tilt up
6. Conclude slow tilt up
7. Initiate slow tilt down
8. Conclude slow tilt down
9. Stand up
10. Transition back to supine
11. Initiate and conclude rapid tilt up
12. Initiate and conclude rapid tilt down
13. Initiate slow tilt up
14. Conclude slow tilt up

15. Initiate slow tilt down
16. Conclude slow tilt down

8. Record 12821

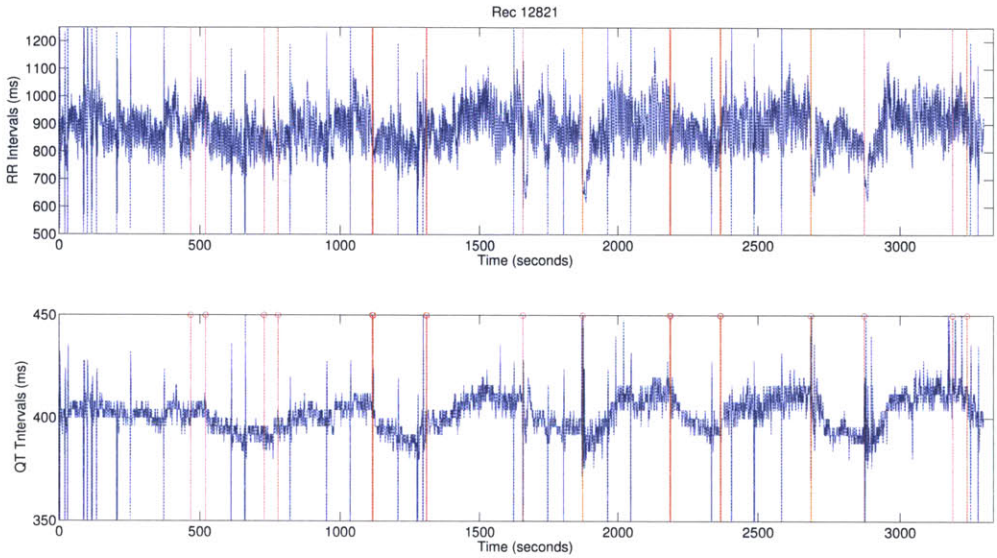

Figure A.8: 12821

Annotations for Figure A.8

1. Initiate slow tilt up
2. Conclude slow tilt up
3. Initiate slow tilt down
4. Conclude slow tilt down
5. Initiate and conclude rapid tilt up
6. Initiate and conclude rapid tilt down
7. Stand up
8. Transition back to supine

9. Initiate and conclude rapid tilt up
10. Initiate and conclude rapid tilt down
11. Stand up
12. Transition back to supine
13. Initiate slow tilt up
14. Conclude slow tilt up
15. Initiate slow tilt down
16. Conclude slow tilt down

9. Record 13960

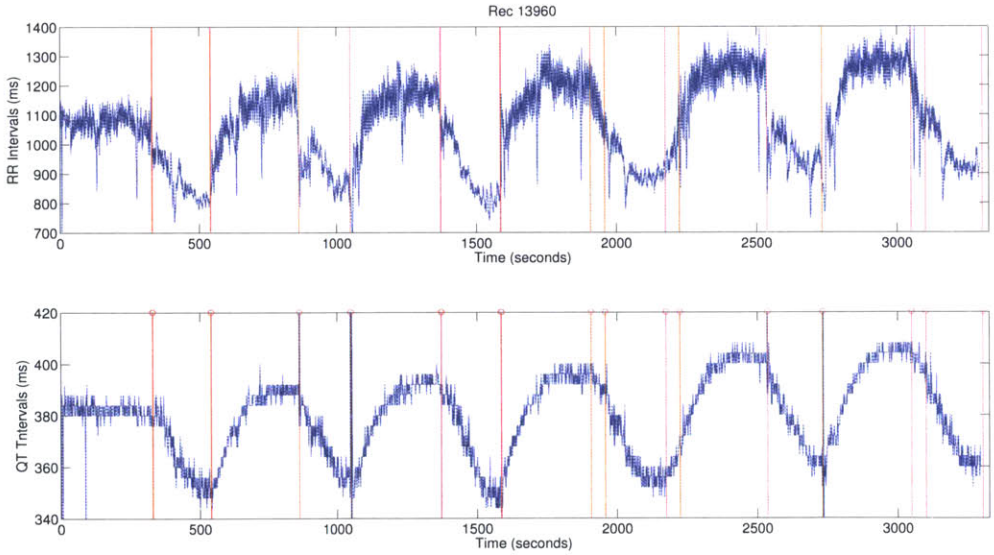

Figure A.9: 13960

Annotations for Figure A.9

1. Initiate and conclude rapid tilt up
2. Initiate and conclude rapid tilt down

3. Stand up
4. Transition back to supine
5. Initiate and conclude rapid tilt up
6. Initiate and conclude rapid tilt down
7. Initiate slow tilt up
8. Conclude slow tilt up
9. Initiate slow tilt down
10. Conclude slow tilt down
11. Stand up
12. Transition back to supine
13. Initiate slow tilt up
14. Conclude slow tilt up
15. Initiate slow tilt down
16. Conclude slow tilt down

■ A.2 RR, QT and QTc Intervals

The figures below show RR, QT and corrected QT intervals. The corrections used here are the Bazett formula, $QT_c = \frac{QT}{\sqrt{RR}}$ and the Federica cube root formula, $QT_c = \frac{QT}{\sqrt[3]{RR}}$.

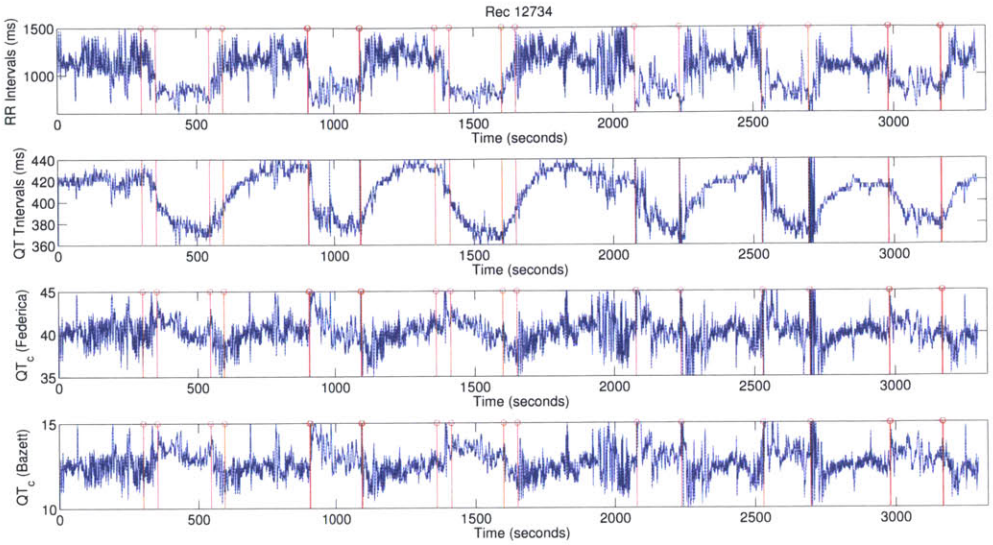

Figure A.10: 12734 showing QT interval corrections

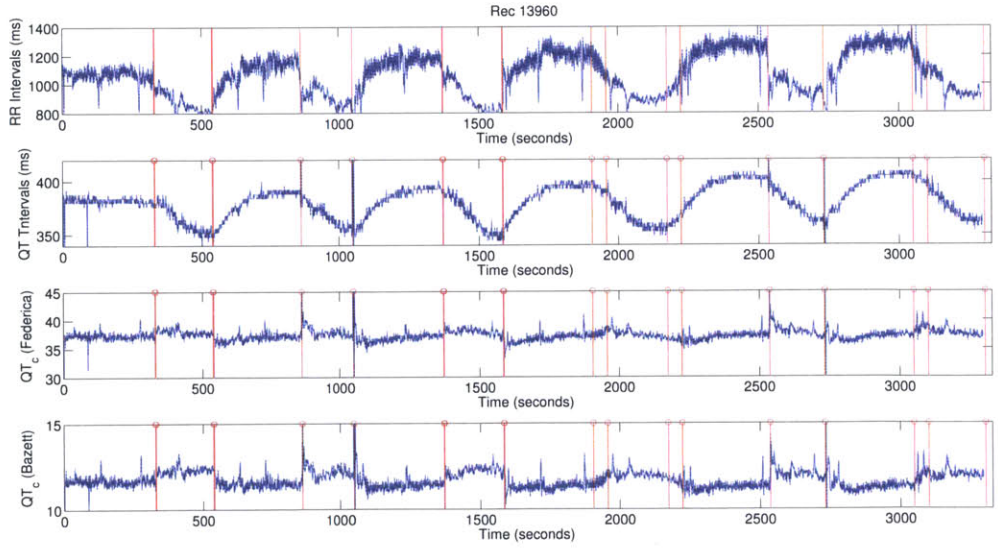

Figure A.11: 13960 showing QT interval corrections

Appendix B

Spectral Analysis of Tilt Table Data

These are some examples of power spectral density and residual error spectrum plots derived from the tilt table data. These plots are from subject 12344 before and after the interventions in the tilt table experiment.

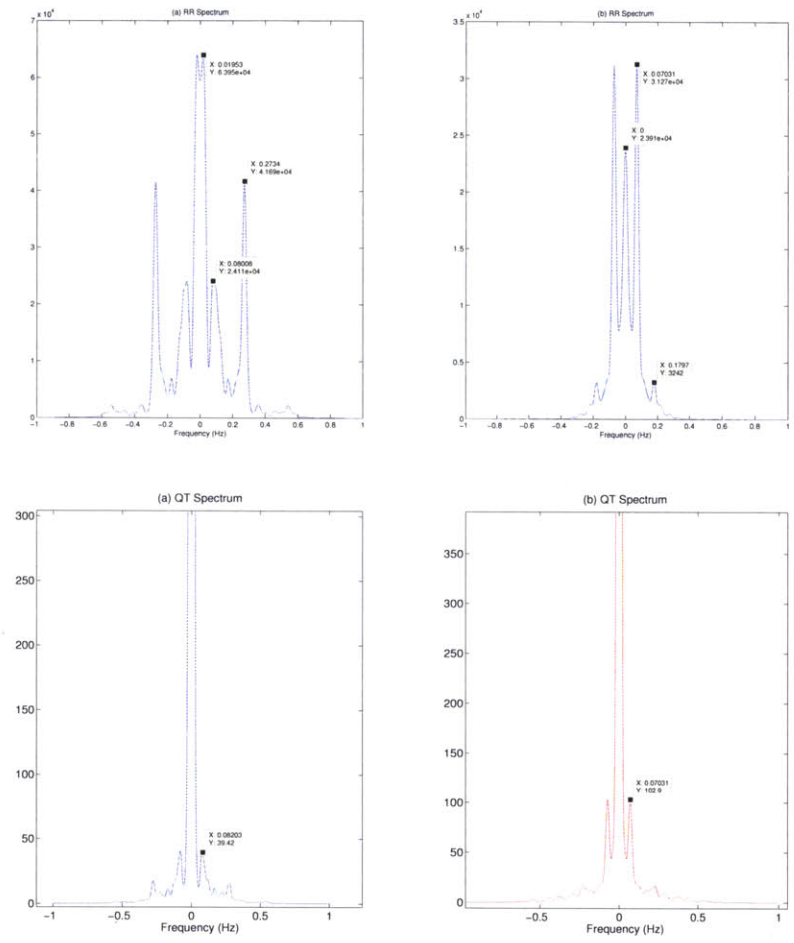

Figure B.1: From L-R: PSD before and after second slow tilt up of 12734. Time series shown in figure 5.4 RR PSD *(top)* and QT PSD *(bottom)*.

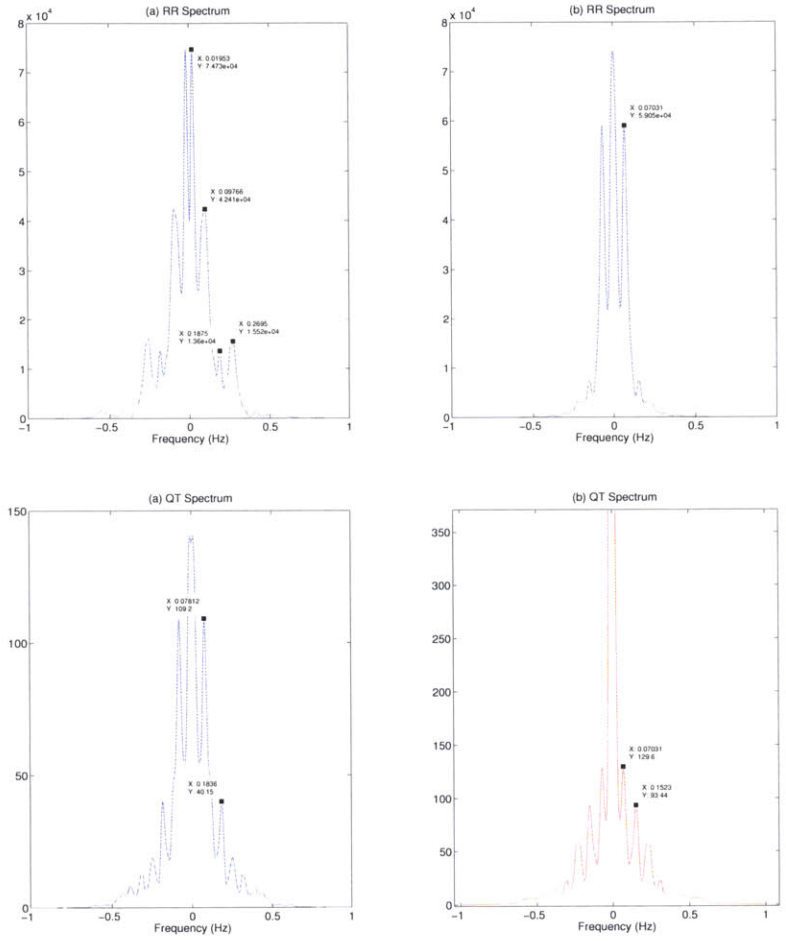

Figure B.2: From L-R: PSD before and after first rapid tilt up of 12734. Time series shown in the top plots of Figure 5.4. RR PSD *(top)* and QT PSD *(bottom)*.

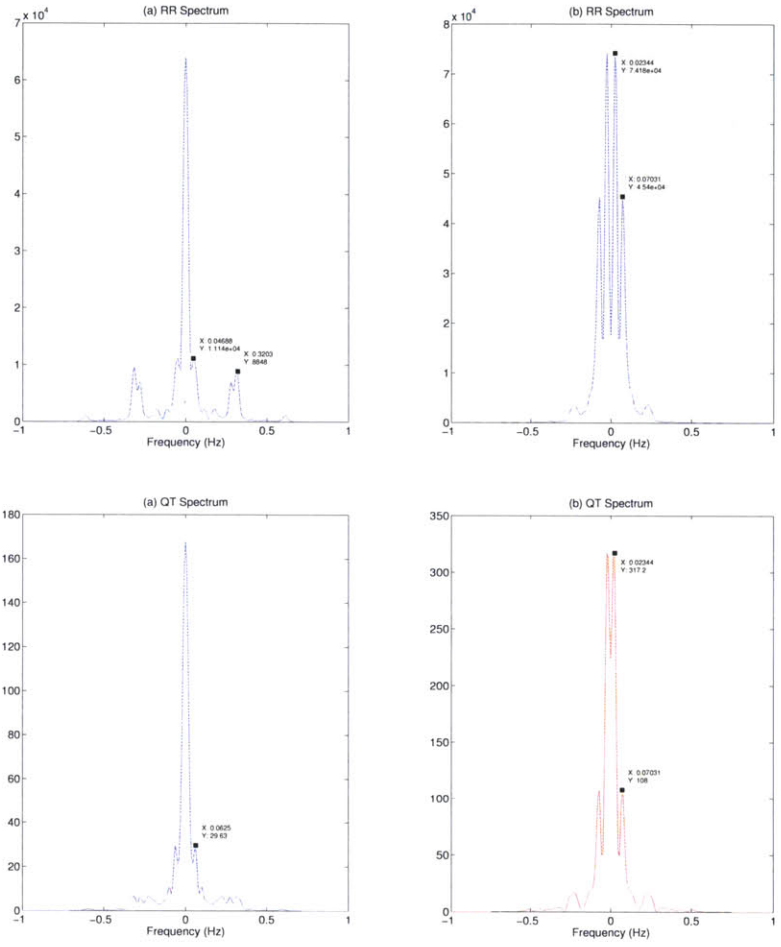

Figure B.3: From L-R: PSD before and after second rapid tilt up of 12734. Time series shown in the top plots of Figure 5.3. RR PSD *(top)* and QT PSD *(bottom)*.

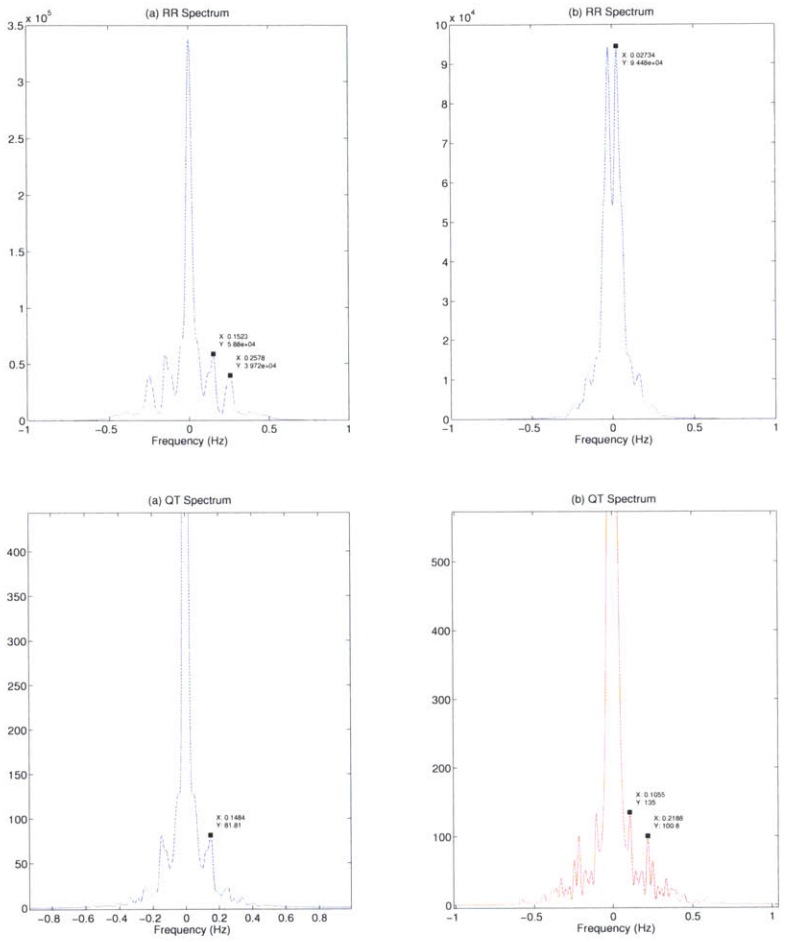

Figure B.4: From L-R: PSD before and after first stand up of 12734. Time series shown in the top plots of Figure 5.5. RR PSD *(top)* and QT PSD *(bottom)*.

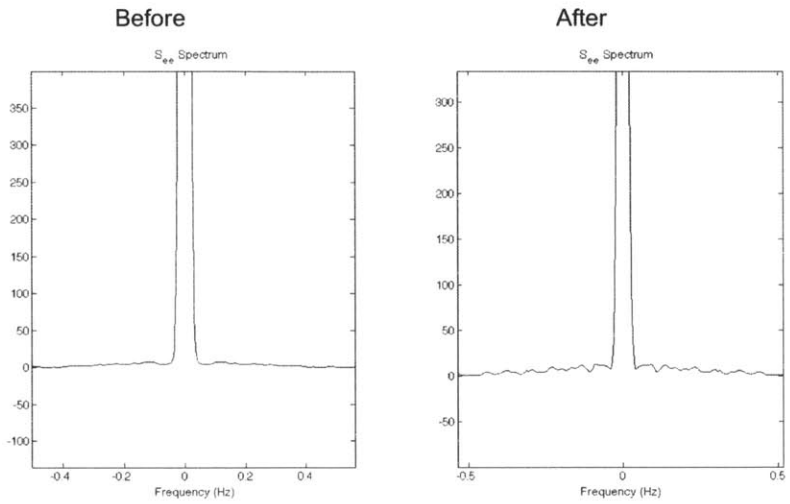

Figure B.5: Residual error spectrum of second slow tilt-up of record 12734

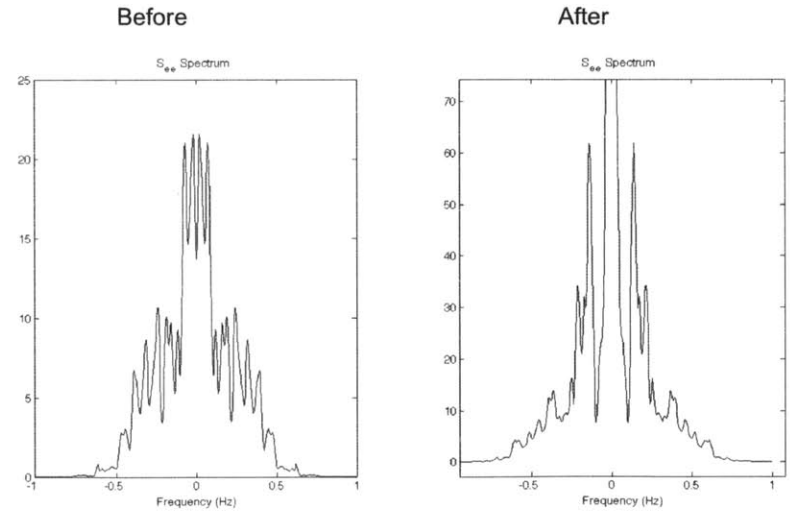

Figure B.6: Residual error spectrum of first rapid tilt-up of record 12734

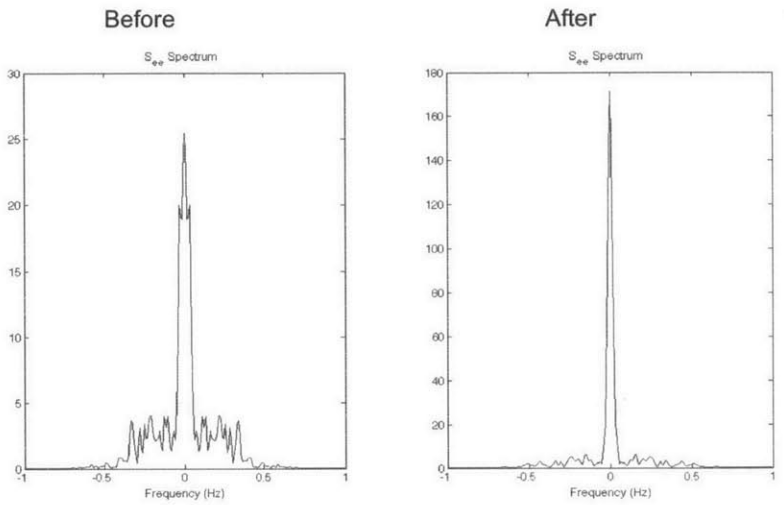

Figure B.7: Residual error spectrum of second rapid tilt-up of record 12734

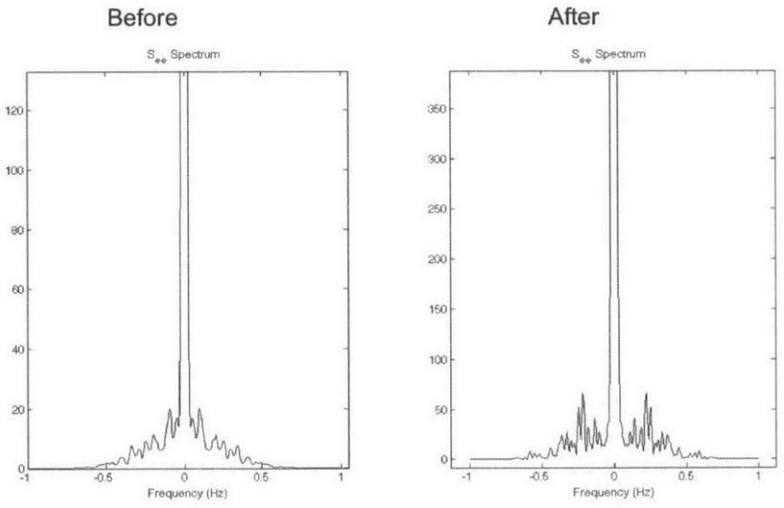

Figure B.8: Residual error spectrum of first stand-up from supine of record 12734

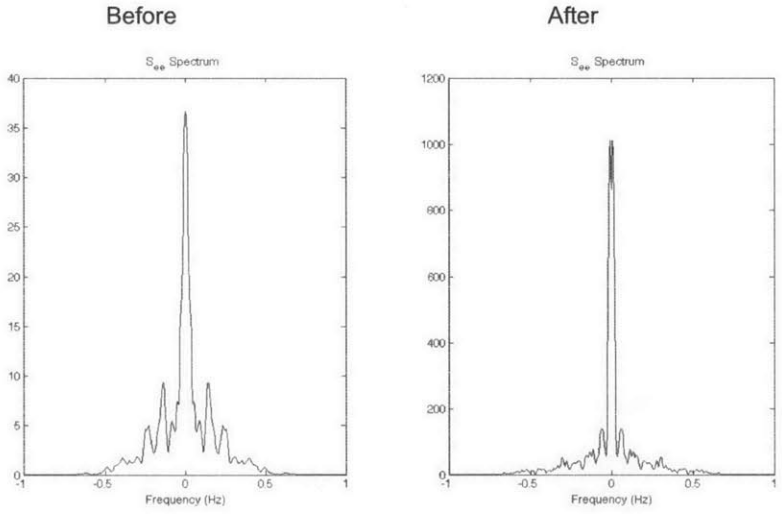

Figure B.9: Residual error spectrum of second stand-up from supine of record 12734

Appendix C

Exponential Fit Model

$$y(t) = y(t=\infty) - \big(y(t=\infty) - y(t=0)\big)e^{-\lambda t}$$

where $\lambda = \frac{1}{\tau}$

$$\frac{y(t=\infty) - y(t)}{y(t=\infty) - y(t=0)} = e^{-\lambda t}$$

Taking logs,

$$\ln\big(y(t=\infty) - y(t)\big) - \ln\big(y(t=\infty) - y(t=0)\big) = -\lambda t$$

Let the lefthand side of the above equation be $r(t)$, then the least squares estimate for λ is

$$\hat{\lambda} = -\frac{\sum_i r(t_i)t_i}{\sum_i t_i^2}$$

The estimated curve, $y(t)$ becomes,

$$\hat{y}(t) = y(t=\infty) - \big(y(t=\infty) - y(t=0)\big)e^{-\hat{\lambda} t}$$

Bibliography

[1] S. Akselrod, D. Gordon, F. A. Ubel, and D. C. Shannon. Power spectrum analysis of heart rate fluctuation: a quantitative probe of beat-to-beat cardiovascular control. *Science*, 213:220–222, 1981.

[2] S. M. Al-Khatib, N. M. LaPointe, J. M. Kramer, and R. M. Califf. What clinicians should know about the QT interval. *JAMA: The Journal of the American Medical Association*, 289(16):2120–7, 2010.

[3] M. Alghatrif and J. Lindsay. A brief review: history to understand fundamentals of electrocardiography. *Journal of Community Hospital Internal Medicine Perspectives*, 2(1):1–5, January 2012.

[4] F. Badilini, P. Maison-Blanche, R. Childers, and P. Coumel. QT interval analysis on ambulatory electrocardiogram recordings: a selective beat averaging approach. *Medical and Biological Engineering and Computing*, 37(1):71–9, January 1999.

[5] R. D. Berger. QT interval variability: is it a measure of autonomic activity? *Journal of the American College of Cardiology*, 54(9):851–2, August 2009.

[6] R. D. Berger, E. K. Kasper, K. L. Baughman, E. Marban, H. Calkins, and G. F. Tomaselli. Beat-to-beat QT interval variability: novel evidence for repolariza-

tion lability in ischemic and nonischemic dilated cardiomyopathy. *Circulation*, 96(5):1557–1565, September 1997.

[7] R.D. Berger, S. Akselrod, and D. Gordon. An efficient algorithm for spectral analysis of heart rate variability. *IEEE Transactions on Biomedical Engineering*, BME-33(9):900–904, 1986.

[8] R. S. Bexton, H. O. Vallin, and A. J. Camm. Diurnal variation of the QT interval-influence of the autonomic nervous system. *British Heart journal*, 55(3):253–8, March 1986.

[9] G. Casolo, E. Balli, T. Taddei, J. Amuhasi, and C. Gori. Decreased spontaneous heart rate variability in congestive heart failure. *The American Journal of Cardiology*, 64(18):1162–1167, November 1989.

[10] L. S. Constanzo. *Physiology.* Elsevier/Saunders, 4th edition, 2010.

[11] D. J. Ewing, J. M. Neilson, C. M. Shapiro, J. A. Stewart, and W. Reid. Twenty four hour heart rate variability: effects of posture, sleep, and time of day in healthy controls and comparison with bedside tests of autonomic function in diabetic patients. *British Heart Journal*, 65(5):239–44, May 1991.

[12] A. L. Goldberger, L. A. N. Amaral, L. Glass, J. M. Hausdorff, P. Ch. Ivanov, R. G. Mark, J. E. Mietus, G. B. Moody, C-K. Peng, and H. E. Stanley. PhysioBank, PhysioToolkit, and PhysioNet: components of a new research resource for complex physiologic signals. *Circulation*, 101(23):e215 – e220, 2000.

[13] T. Gregory and M. Smith. Cardiovascular complications of brain injury. *Continuing Education in Anaesthesia, Critical Care and Pain*, 12(2):67–71, December 2011.

[14] T. Heldt, M.B. Oefinger, and M. Hoshiyama. Circulatory response to passive and active changes in posture. *Computers in Cardiology*, pages 263–266, 2003.

[15] P. Karjalainen, M. Tarvainen, and T. Laitinen. Principal component regression approach for QT variability estimation. *Conference Proceedings of the International Conference of IEEE Engineering in Medicine and Biology Society*, 2:1145–7, January 2005.

[16] J. Keener and J. Sneyd, editors. *Mathematical physiology II: systems physiology*, volume 8/2 of *Interdisciplinary Applied Mathematics*. Springer New York, New York, NY, 2009.

[17] P. Laguna and R. G. Mark. A database for evaluation of algorithms for measurement of QT and other waveform intervals in the ECG. *Computers in Cardiology*, 24:673–676, 1997.

[18] C. P. Lau, A. R Freedman, S. Fleming, M. Malik, A. J. Camm, and D. E. Ward. Hysteresis of the ventricular paced QT interval in response to abrupt changes in pacing rate. *Cardiovascular Research*, 22(1):67–72, January 1988.

[19] M. Malik. Problems of heart rate correction in assessment of drug-induced QT interval prolongation. *Journal of Cardiovascular Electrophysiology*, 12(4):411–420, April 2001.

[20] M. Malik. Beat-to-beat QT variability and cardiac autonomic regulation. *American Journal of Physiology. Heart and Circulatory Physiology*, 295(3):H923–H925, September 2008.

[21] M. Malik and A. J. Camm. Components of heart rate variability-what they really mean and what we really measure. *The American Journal of Cardiology*, 72(11):821–2, October 1993.

[22] A. Mortara, M. T. La Rovere, M. G. Signorini, P. Pantaleo, G. Pinna, L. Martinelli, C. Ceconi, S. Cerutti, and L. Tavazzi. Can power spectral analysis of heart rate variability identify a high risk subgroup of congestive heart failure patients with excessive sympathetic activation? A pilot study before and after heart transplantation. *British Heart Journal*, 71(5):422–30, May 1994.

[23] A. Murray, N. B. McLaughlin, J. P. Bourke, J. C. Doig, S. S. Furniss, and R. W. Campbell. Errors in manual measurement of QT intervals. *British Heart Journal*, 71(4):386–90, April 1994.

[24] L. H. Opie. *The heart: physiology from cell to circulation.* Lippincott WIlliams and Wilkins, 3rd edition, 1998.

[25] S. Oppenheimer. The broken heart: noninvasive measurement of cardiac autonomic tone. *Postgraduate Medical Journal*, 68(806):939–41, December 1992.

[26] M. Pagani, F. Lombardi, and S. Guzzetti. Power spectral analysis of heart rate and arterial pressure variabilities as a marker of sympatho-vagal interaction in man and conscious dog. *Circulation*, pages 178–193, 1986.

[27] M. Pagani, G. Malfatto, S. Pierini, R. Casati, A. M. Masu, M. Poli, S. Guzzetti, F. Lombardi, S. Cerutti, and A. Malliani. Spectral analysis of heart rate variability in the assessment of autonomic diabetic neuropathy. *Journal of the Autonomic Nervous System*, 23(2):143–153, August 1988.

[28] A. Pipilis, M. Flather, O. Ormerod, and P. Sleight. Heart rate variability in acute myocardial infarction and its association with infarct site and clinical course. *The American Journal of Cardiology*, 67(13):1137–9, May 1991.

[29] A. Porta, E. Tobaldini, T. Gnecchi-Ruscone, and N. Montano. RT variability unrelated to heart period and respiration progressively increases during graded

head-up tilt. *American Journal of Physiology. Heart and Circulatory Physiology*, 298(5):H1406–14, May 2010.

[30] A. Porta, E. Tobaldini, V. Magagnin, T. Bassani, T. Gnecchi-Ruscone, and Nicola Montano. Open loop linear parametric modeling of the QT variability. *Annual International Conference of the IEEE Engineering in Medicine and Biology Society*, 2009(5):6453–6, January 2009.

[31] E. Pueyo, P. Smetana, K. Hnatkova, P. Laguna, and M. Malik. Time for QT adaptation to RR changes and relation to arrhythmic mortality reduction in amiodarone-treated patients. *Computers in Cardiology*, pages 565–568, 2002.

[32] M. Quintana, N. Storck, L. E. Lindblad, K. Lindvall, and M. Ericson. Heart rate variability as a means of assessing prognosis after acute myocardial infarction. *European Heart Journal*, pages 789–797, 1997.

[33] M. L. Soria, J. P. Martinez, and P. Laguna. A multilead wavelet-based ECG delineator based on the RMS signal. *Computers in Cardiology*, pages 153–156, 2006.

[34] European task force. Guidelines: heart rate variability. *European Heart Journal*, 17:354–381, 1996.

[35] P. Welch. The use of fast Fourier transform for the estimation of power spectra: a method based on time averaging over short, modified periodograms. *IEEE Transactions on Audio and Electroacoustics*, AU-15(2):70–73, 1967.

[36] W. Zong. A robust open-source algorithm to detect onset and duration of QRS complexes. *Computers in Cardiology*, pages 737–740, 2003.

[37] W. Zong, M. Saeed, and T. Heldt. A QT interval detection algorithm based on

ECG curve length transform materials and methods. *Computers in Cardiology*, 30:737–740, 2003.

[38] G. Zuanetti, J. M. M. Neilson, R. Latini, E. Santoro, A. P. Maggioni, and D. J. Ewing. Prognostic significance of heart rate variability in post myocardial infarction patients in the fibrinolytic era: the GISSI-2 results. *Circulation*, 94(3):432–436, August 1996.